UCRL 10429

University of California

Ernest O. Lawrence Radiation Laboratory

ATOMIC CAPTURE OF μ^- MESONS IN CHEMICAL COMPOUNDS AND THE "FERMI-TELLER Z LAW"

Berkeley, California

DISCLAIMER

UCRL-10429
UC-4 Chemistry
TID-4500 (17th Ed.)

UNIVERSITY OF CALIFORNIA

Lawrence Radiation Laboratory
Berkeley, California

Contract No. W-7405-eng-48

ATOMIC CAPTURE OF μ^- MESONS IN CHEMICAL COMPOUNDS AND THE "FERMI-TELLER Z LAW"

Jagdish S. Baijal

(Thesis)

August 20, 1962

Printed in USA. Price $2.00. Available from the
Office of Technical Services
U. S. Department of Commerce
Washington 25, D.C.

ATOMIC CAPTURE OF μ^- MESONS IN CHEMICAL COMPOUNDS AND THE "FERMI-TELLER Z LAW"

Contents

THIS PAGE

WAS INTENTIONALLY

LEFT BLANK

ATOMIC CAPTURE OF μ^- MESONS IN CHEMICAL COMPOUNDS AND THE "FERMI-TELLER Z LAW"

Jagdish S. Baijal

Lawrence Radiation Laboratory
University of California
Berkeley, California

August 20, 1962

ABSTRACT

We describe experimental studies of the relative atomic μ^--meson capture probabilities in the constituents of chemical compounds. Fermi and Teller had predicted that the atomic-capture probability is proprotional to the nuclear charge of the atomic species weighted by its atomic concentration. This is sometimes referred to as the "Fermi-Teller Z law." Previous experiments have indicated no clear systematics to this capture process and there are conflicts between the results of several measurements made with the same or similar compounds. In these experiments the capturing atom has been identified by detection of either mesic x rays or decay electrons from μ^- mesons bound in the atoms mesic K shell in the atomic species. In our experiment we are concerned with oxides and sulfides of some medium- and high-Z elements as well as two metallic solutions, and we detect a nuclear capture product, neutron, rather than the decay electrons. Our results show that among the substances examined--namely CuO, Sb_2O_3, PbO, CuS, Sb_2S_3, PbS, AgLi, and CuAu-- the "Z law" behavior is not indicated either in insulators or in metals, although in all cases there is a preference for capturing in the atom of higher Z.

Suppose the atomic-capture probability is proportional to Z^n (n being any positive or negative number), then we find that our experimental results fall approximately in the range $n = 2/3$ to $n = 1.4$, where $n = 1$ would define the prediction by Fermi and Teller. The measured atomic-capture ratios are: $Cu/O = 6.14 \pm 0.85$; $Sb/O = 1.86 \pm 0.096$; $Pb/O = 4.56 \pm 0.53$; $Cu/S = 1.89 \pm 0.18$; $Sb/S = 1.64 \pm 0.10$; $Pb/S = 2.87 \pm 0.35$; $Ag/Li = 11.66 \pm 3.39$; $Au/Cu = 0.34 \pm 0.032$.

In connection with this experiment it was also necessary to measure the μ^--meson lifetimes in a number of elements (including Au, which has not been reported before). The measured lifetimes are (in nsec): S = 498± 17; Cu = 162.6± 1.9; Ag = 84.4± 1.0; Sb = 91.3± 1.4; Au = 68.6± 1.3; Pb = 74.1±1.0.

I. INTRODUCTION

A. Atomic Capture of μ^- Mesons

Tomonaga and Araki were the first to point out the effect of the Coulomb field of the nucleus on the behavior of a slow charged meson.[1] They indicated that the repulsive field of the positively charged nucleus would prevent a positively charged meson from approaching the nucleus. Thus the positively charged meson would be forced to roam about in matter and ultimately decay. But a slow negative meson would be attracted to the nucleus and undergo nuclear absorption. When the μ^- meson stops in matter, it initially loses its energy by ionization as it slows down and then finally is trapped in a Bohr orbit about a nucleus. Then it cascades down to a K orbit, emitting Auger electrons and mesic x rays. Once the μ^- meson reaches the K orbit, it either decays or interacts with the nucleus. The classic experiment of Conversi, Pancini, and Piccioni gave the first evidence of this competition between decay and capture.[2] The experiment consisted of stopping μ^- mesons in carbon as well as in iron, and observing the decay electrons. They observed decay electrons from μ^- stoppings in carbon but almost no decay electrons from iron. In later experiments the lifetimes were measured over a wide spectrum of atomic numbers.[3,4,5] These experiments were found to be quite compatible with the hypothesis of nuclear absorption competing with the decay.

The π mesons or μ mesons are unstable particles. A requirement for the negative π or μ mesons to be absorbed by the nucleus is that the time taken by them to reach the mesic K shell of the atom should be less than their mean lifetime. Fermi and Teller were the first to point out that the time taken by the π or μ meson to slow down and be captured is much shorter than its decay time.[6] Assuming the Fermi-Thomas model for the electrons, Fermi and Teller calculated that the total time taken by a meson to be slowed down and captured and to cascade down to the K orbit is of the order of 10^{-13} sec, which is much shorter than the decay time of either the π^- or μ^- meson, thus ensuring the existence of mesonic atoms.

Fermi and Teller also considered the slowing down and capture process in a homogeneous chemical mixture. They calculate that the probability for capture of a muon by an atom is proportional to the energy loss of the muon near that nucleus. From this they concluded that the relative atomic-capture probability of muons in different elements in a compound should be proportional to the nuclear charge of the atomic species weighted by its atomic concentration. This is sometimes referred to as the "Fermi-Teller Z Law."

During the past years a number of experiments have been reported in the literature concerning the relative atomic-capture probabilities of μ^- mesons in insulators and metal.[7-13] The results of these experiments, in which the same or similar compounds were used, are in disagreement with each other as well as with the predictions of Fermi and Teller. In the present experiment we describe a study of these atomic capture ratios for different compounds having a wide range for the ratio of the atomic numbers of the constituent elements in a compound. In addition to the purely theoretical interest in atomic-capture processes, such information is also needed in the interpretation of various experimental results obtained with nuclear emulsions, compound targets, etc., when the μ^- mesons are brought to rest in such compounds and mixtures. For the interpretation of their results, previous workers have relied on the theoretical conjecture of Fermi and Teller which does not seem to hold good.[14]

B. Capture in Compounds

Panofsky et al. determined the mass of π^0 mesons by studying π^- absorption in hydrogen.[15] When they used LiH and CH_2 targets, they found none of the gamma rays that accompany absorption by a proton and inferred that all the π^- mesons were captured in lithium and carbon, and none in hydrogen. This is known as the Panofsky effect. This was, however, not surprising. It had been pointed out by Fermi and Teller in their paper that any meson orbital captures in hydrogen would create a small neutral system that could permeate the lattice. The result is that mesons would eventually be transferred to a more highly charged nucleus.

The experiment of Stearns and Stearns was the first specifically designed to determine the relative atomic-capture probability of negative mesons in compounds.[7] In their measurements they compared the relative yields of mesic x rays for a substance in the form of a compound and for a mixture having the same composition. For a mixture they assumed that the ordinary ionization-loss formula would govern the stopping power and thereby the amount of capture in each element. They assumed that the stopping power per atom was proportional to Z, and therefore that the amount of capture in each element of a macroscopic mixture would go as Z times atomic concentration. They compared the x-ray yields of π^--mesonic L and M lines from a CaS compound and a mixutre of the two elements. They found the relative yields to be the same within 5%. Similarly they studied the μ^--mesonic x rays, using Al_2O_3 and a mixture of Al and H_2O (which is equivalent to oxygen because of the Panofsky effect). The yields for the mixture and the compound were again found to be identical within 5%. Using these results and assuming that the capture in the compound depends upon Z^n, Stearns and Stearns found $n = 1 \pm 0.20$ for CaS and $n = 1.0 \pm 0.1$ for Al_2O_3. On the basis of these results they showed that the relative atomic captures in a compound are proportional to Z, and therefore are in accordance with the predictions of Fermi and Teller.

These results have been criticized by Sens et al.,[8] who argue that the atomic stopping power for low-energy mesons is not given by the ordinary ionization-loss formula as was assumed by Stearns and Stearns. If we look at the range-energy tables of Rich and Madey,[9] we find that for low-energy mesons of the order of 1 MeV or so, the stopping power of oxygen is more than that of Al. The atomic stopping power is not known accurately at low energies.

Sens et al. have also looked into this problem.[8] They stopped mesons in compounds and measured the decay curves by detecting decay electrons with a counter telescope. Knowing the mean lifetime of μ^- mesons in each constituent of a compound and the branching

ratio between decay and capture, they unfolded the composite decay curve. From it they were able to get the relative number of μ^- mesons reaching the mesic K shell in the constituents of a compound.

The methods of Stearns and Stearns, and that of Sens et al., however, differ from each other. In the former, the elements in a compound are identified by their K and L series etc., for mesonic x rays, while the latter distinguishes the same elements by the different lifetimes of mesons in these elements.

Sens et al. report that their results agree much better with the capture occurring in proportion to the number of atoms of each constituent than with the predictions of Fermi and Teller. These results, together with the results of other workers to be mentioned later, are given in Table I.

The results of Sens et al. indicate that for the oxide compounds the captures in oxygen are consistently higher than the captures according to the calculations of Fermi and Teller. The captures are in fact not given by the atomic ratios either. This can be seen from the results as given in Table I (as well as from the plot in Fig. 24).

Various other workers--Backenstoss et al.,[12] Lathrop et al.,[10] Astbury et al.,[11] and Eckhause et al.[13]--have studied this problem of μ^- captures in different chemical compounds.

Backenstoss et al. showed, on the basis of their experiment in the compounds LiH, AgCl, and UF_4, that their results for μ^- captures indicate violations of the Z law similar to those observed by Sens et al. Their method consisted in finding the decay curves characteristic of the decay of μ^- mesons captured in Li, Cl, and F in those compounds. This was done by detecting the decay electrons.

Lathrop et al. later retested the compound LiI. They found that the experimental result agrees with the Z dependence rather than with the atomic ratio. This result is in striking contradiction with the results of Backenstoss et al. It may be worth pointing out that the final results given by Lathrop et al. are obtained only after applying rather large corrections. For I/Li they obtained 10.5 ± 1.3. After

Table I. Summary of "Z law" results from previous workers. Relative numbers of μ^- mesons reaching the 1S level in the constituents of a compound.

Compound	Ratio	Observed	Predicted, Fermi and Teller	Atomic ratio	n†
Sens et al. (Chicago)					
P_2O_5	P/O	0.371±0.041	0.75	0.4	-0.12±0.18
Al_2O_3	Al/O	0.435±0.038	1.084	0.66	-0.88±0.18
SiO_2	Si/O	0.386± 0.025	0.875	0.5	-0.46±0.12
KOH	K/O	0.455±0.083	2.38	1.0	-0.91±0.21
KHF_2	K/F	0.588±0.138	1.053	0.5	0.19±0.27
$C_6H_4Cl_2$ (Liquid)	Cl/C	0.435±0.0378	0.943	0.33	0.27±0.083
$C_6H_4Cl_2$ (Solid)	Cl/C	0.476±0.045	0.943	0.33	0.35±0.091
CCl_4	Cl/C	4.1±0.8	11.3	4.0	0.024±0.19
Lathrop et al. (Chicago)					
LiI	I/Li	15.8±2.0	17.67	1	0.96±0.044
AgZn	Ag/Zn	2.2±0.7	1.57	1	1.75±0.71
Astbury et al. (Liverpool)					
PbF_2	Pb/F	4.8±0.7	4.5	0.5	1.02±0.07
Backenstoss et al. (Carnegie Tech.)					
AgCl	Ag/Cl	0.8±0.2	2.8	1	-0.22±0.24
LiI	I/Li	1.3±0.5	17.67	1	0.091±0.13
UF_4	U/F	0.7±0.3	2.6	0.25	0.44±0.18
Eckhause et al. (Carnegie Tech.)					
BiF_3	Bi/F	1.58±0.15	3.07	0.33	0.70±0.043
UF_4	U/F	1.52±0.15	2.56	0.25	0.78±0.043
$CuAl_2$	Cu/Al	1.75±0.18	1.11	0.5	1.56±0.13

† Assuming that the atomic capture probability goes as Z^n (n being any positive or negative number), we have calculated n for these compounds.

applying the correction for the decays from stops in the container walls, they obtained the final ratio I/Li = 15.8±2.0, which is in agreement with the calculations of Fermi and Teller.

The experiment of Astbury et al. with PbF_2 shows an agreement with the Z law behavior rather than with atomic ratio.

The results of Eckhause et al. for BiF_3 and UF_4 also indicate that there are enhanced captures in fluorine (the lower Z constituent), more than the Z law would predict. Their results are also not approximated by the atomic ratios either, but lie between the atomic ratios and the Z law.

Lathrop et al. have studied the atomic μ^- captures in an AgZn alloy which seems to indicate a Z law behavior. However, a recent study of a $CuAl_2$ alloy by Eckhause et al. shows a disagreement with the predictions by Fermi and Teller of the direction of enhanced capture in the heavier element. The results for AgZn by Lathrop et al., as Eckhause et al. point out, though compatible with the Fermi-Teller prediction, are not in disagreement with their result for $CuAl_2$ alloy in view of the magnitudes of the uncertainties. This can be seen from the values of n for these alloys as given in Table I.

We also have measured the atomic μ^- capture in metallic compounds, CuAu and AgLi, which we report in this thesis (Sec. VII, Table V).

C. Present Experiment

In view of the conflicting evidence among experimental results and the absence of any apparent systematic relationship governing the μ^- meson captures, we have carried out our experiment using a technique different from any previously employed.

The previous investigations, as mentioned earlier, have been done by the detection of decay electrons or mesic x rays. These experiments suffer from the following disadvantages. In low-Z nuclei, the decay rate of muons exceeds the capture rate. Therefore the presence of any low-Z material in the immediate neighborhood is a

source of a relatively large number of electrons (for example, carbon in the scintillation counter). If the detected product is a nuclear gamma ray, then a single detector rather than a counter telescope is used. This detector is then sensitive to the bremsstrahlung background as well as to the "zero time" background produced by mesic x rays.

Therefore, we detect capture neutrons, rather than decay electrons or mesic x rays, in our investigation of the relative atomic-capture probability of μ^- mesons in the constituents of a compound. For elements of Z greater than 10, the yield for capture products exceeds that for the decay products. There is very little background effect caused by mesons stopping in the counter or in the container walls because of their low values of Z.

The choice of targets was governed by the following considerations:

(1) The ratio of the atomic numbers of the two elements in the compound should differ sufficiently so that the lifetimes of the μ^- mesons could be clearly distinguished. The ratios of the atomic members covered a wide range so that the overall effect of these ratios on the μ^- capture could be seen. In our experiment, the ratios varied between two and sixteen.

(2) We chose different binary compounds of the same element when the other constituent varied greatly in Z.

(3) We chose oxides, since the previous work of Sens et al. included several oxides, all of which indicated enhanced captures in oxygen.

(4) We also chose several sulfide compounds because the oxides complement the sulfides as regards chemical similarity but are different in Z. Oxygen and sulfur have the same electron configurations in their outer energy levels. It is these outer levels which determine the chemistry, since it is they which interact when atoms approach one another.

In connection with this experiment, it was also necessary to measure μ^--meson lifetimes in a number of elements--namely, S, Cu, Ag, Sb, Au, and Pb. These measured lifetimes are of comparable or greater statistical accuracy than the measurements

previously reported by other experimenters. (Au has not been reported previously.) The measured lifetimes are given in Appendix B. The capture rates calculated from these are least-squares-fitted to Primakoff's formula.[16]

II. THEORY

In this section we outline the theoretical work of Fermi and Teller on the atomic capture of μ^- mesons in compounds. To discuss their work, we have to consider the slowing down of a meson in matter. By studying this process, we can then discuss how the physical and chemical states of matter may influence the capture process.
As long as the velocity of the muon is greater than the orbital velocity of the electrons (2000 eV) the slowing-down process takes place in the same way as for the fast heavy particles. The energy loss per unit time is given by

$$-\frac{dW}{dt} = \frac{4\pi e^4 NZ}{mV} \ell n\left(\frac{b_{max}}{b_{min}}\right) , \qquad (1)$$

where W is the energy of the muon, V its velocity, m the electron mass, N the number of atoms with atomic number Z per cubic cm, and b_{max} and b_{min} the extreme values of the collision parameters. The logarithmic factor becomes zero when the velocity of the meson becomes equal to the velocity of the electron.

When the velocity of the meson is less than that corresponding to a kinetic energy of 2000 eV, expression (1) does not describe correctly the energy loss of the mesons. To calculate it, Fermi and Teller assumed that the mesons are moving inside a degenerate electron gas. Suppose V, the velocity of the mesons, is less than v_0, the Fermi limit velocity of the electrons. Then, since V is less than v_0, the meson can interact only with those electrons whose velocities are between $v_0 - V$ and v_0, because of the Pauli exclusion principle. So we can write, for the energy loss per unit time of the meson,

$$-\frac{dW}{dt} = n\sigma v_0 W , \qquad (2)$$

where n is the number of electrons per cubic cm that can collide with the meson, σ is the electron-meson collision cross section for

large deflections, and W is the average energy transferred in collisions of this type.

We can estimate roughly the quantities on the right-hand side of Eq. (2). When V is small compared with v_0, we can write

$$n \approx \frac{m^3 v_0^2}{\hbar^3} V ,$$

$$\sigma \approx \left(\frac{e^2}{m v_0^2} \right)^2 ,$$

$$W \approx m v_0 V ,$$

so

$$-\frac{dW}{dt} \approx W \sigma n v_0$$

$$\approx \frac{m^2 e^4 v^2}{\hbar^3}$$

$$\approx \frac{m^2 e^4 T}{(\mu \hbar^3)}$$

$$\approx \frac{T}{t_0} , \qquad (3)$$

where T is the kinetic energy of the meson, $t_0 = \frac{\mu \hbar^3}{m^2 e^4} = 4.84 \times 10^{-15}$ sec is the characteristic time for the process, and μ is the mass of the meson. A more exact calculation has also been made by Fermi and Teller; however, for estimates of this order of magnitude, Eq. (3) is sufficient.

To calculate the rate of energy loss in this region, we have to find the average value $\overline{T}$ of the kinetic energy T in Eq. (3).

The average kinetic energy $\overline{T}$ is given by

$$\overline{T} = \frac{\int (W-U)^{3/2} d\tau}{\int (W-U)^{1/2} d\tau} , \tag{4}$$

where U is the potential energy, $d\tau$ is the volume element, and W is the total energy. In finding the average, Fermi and Teller supposed that the probability of finding the meson in a given volume element is weighted by the phase space available to it.

For W greater than U, $\overline{T}$ is equal to W. Near zero energy the meson cannot pass from one atom to another. In such a case U is no longer negligible and so $\overline{T}$ is appreciably larger than W. When W is negative, then the kinetic energy is of the order of the absolute value of W.

Fermi and Teller used for the potential U the value obtained from the statistical model, namely

$$U = - \frac{Z^{4/3} e^2}{b} \frac{\phi(x)}{x} , \tag{5}$$

where x is related to the distance from the nucleus by the relation $V = xbZ^{-1/3}$ and the length $b = 0.47 \times 10^{-8}$ cm. The function $\phi(x)$ has been tabulated by Fermi.[17]

From Eqs. (4) and (5), Fermi and Teller obtained, for the average kinetic energy $\overline{T}$,

$$\overline{T} = \frac{N^{-1} W^{3/2} + 4\pi Z e^3 b^{3/2} \left(1 - \frac{0.8}{x_0}\right)}{N^{-1} W^{1/2} + 3.96\, e\, b^{5/2} Z^{-1/3} x_0^{\,2}} , \tag{6}$$

where x_0 is given by

$$\frac{1}{N} = \frac{4\pi b^3 x_0^{\,3}}{3Z} , \tag{6a}$$

or

$$dW/dT = \frac{N^{-1}W^{3/2} + 4\pi Z e^3 b^{3/2}(1 - 0.8/x_0)}{N^{-1}W^{1/2} + 3.96\, eb^{5/2} Z^{-1/3} x_0^2} \frac{1}{t_0} \quad . \qquad (7)$$

The case of insulators is different from that of metals. For insulators there are Brillouin gaps. The amount of energy given to the electrons in metals can be arbitrarily small, but in an insulator it has to be at least as large as the Brillouin gap, which is usually a few electron volts.

We have mentioned before that the energy delivered to the electron in a collision is of the order of $mv_0 V$. This means that Eq. (3) for the energy loss per unit time $-\frac{dW}{dt} \approx \frac{\overline{T}}{t_0}$ will be valid only for $mv_0 V > G$, where G is the Brillouin gap, or the minimum energy that the electrons can accept. If the above condition is not obeyed, then the rate of energy loss will be smaller. This condition will have to be taken into account while we carry out the integration in expression (4) for $\overline{T}$.

Fermi and Teller conclude that the effect of this gap is to increase the slowing-down time for μ^- mesons by perhaps 10%.

Fermi and Teller then considered the relative probability for μ^--meson capture by the constituents of the compound. They estimated this to be proportional to the energy loss of the μ^- mesons near that nuclear species. From an expression of type (6), they found it to be proportional to Z. The complete expression from which they deduce the Z law has not been given in detail in the paper. They mention that this energy loss at $W = 0$ is given by an expression whose numerator contains the numerator of (7). For $W = 0$, this is proportional to Z. The denominator of this expression is a constant for all atomic species. (The detailed calculation showing that the denominator is a constant for all atomic species is not given.) However, we notice from Eq. (7) (which seems to this author the correct expression for energy loss near $W = 0$) that at $W = 0$ the denominator is proportional to $Z^{1/3}$ after substituting for x_0 from Eq. (6a). The rate of energy loss is then proportional to $Z^{2/3}$ instead of Z.

III. EXPERIMENTAL ARRANGEMENT

A. The Magnet System and the Beam

The experimental arrangment is shown in Fig. 1. Negative pions were produced by bombarding a 2-in.-thick Be target in the 184-inch cyclotron with 730-MeV protons. Some of these pions immediately decay into muons near the target. These pions and muons are momentum-analyzed by the fringing field and pass out of the cyclotron vacuum tank through a thin aluminum window. The beam then entered the meson cave through an 8-ft-long iron collimator. Focusing and further momentum analysis were provided by an 8-in. quadrupole doublet and a 50-deg bend through an H magnet. The beam then passed through a 4×4-in. aperture in a Pb collimator into a room made from 4-ft thick concrete blocks.

The beam was monitored by a coincidence telescope consisting of two 4×4×1/4-in. plastic scintillators, S_1 and S_2, placed as shown in Fig. 1. The signal from another coincidence telescope, $S_3S_4\overline{AC}$, signified the stopping of a meson in the target. (The bar above a counter symbol means anticoincidence, or that the absence of a pulse was required.) The S_3 and S_4 were plastic scintillators similar in size to S_1 and S_2. The C was a water Cerenkov counter, 5×5×2 in., that served to veto coincidence pulses produced by electrons in the beam. The anti-counter A, vetoed particles that passed through the target without stopping.

Figure 2 shows the relative $S_3S_4\overline{AC}$ counting rate as a function of the thickness of absorber placed between S_2 and C. The momentum of the incident beam was about 200 MeV/c.

Two things were done to minimize the neutron background caused by stopping pions. First, CH_2 was used as the absorbing material to minimize neutron production from π^- stoppings and to act as a moderator for neutrons produced. Second, an effort was made to maximize the μ/π ratio with a minimum loss of μ intensity.

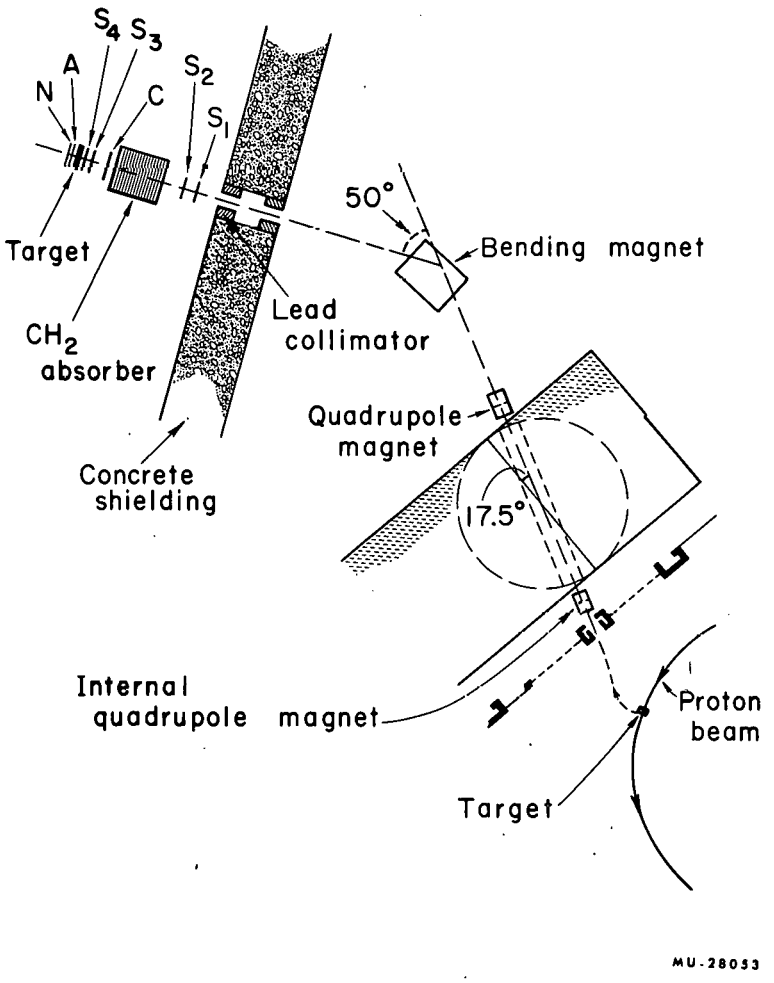

Fig. 1. Experimental arrangement.

The position of the internal Be target was first varied to optimize the total flux through the telescope. The target can be moved both radially and azimuthally by means of external controls.

Then the bending-magnet current was increased about 10%. While reducing somewhat the μ intensity this also increases the μ/π ratio from 1/5 to somewhat better than 3/1. This is because the π source is essentially the size of the target, whereas the μ, being produced in π decay, has a more diffuse source. By detuning the magnet we shift the apparent-source position away from the center of the target. This reduces both the π and μ intensities but the effect on the π's is much greater than on the μ's.

In Fig. 2 we show a differential range curve taken after this adjustment is made. The π^- peak is at 8.5 in. of CH_2 and the μ^- peak at 12.5 in. The stopping rate in a 5-g/cm^2 target over the area defined by the 4×4-in. counter was about 17,000/min.

B. Electronics

A schematic diagram of the electronics is shown in Fig. 4. The signal ($S_3S_4\overline{AC}$), indicating a μ^- stop in the target, is used to generate a "gate pulse" 3 μsec wide through a gate generator, G. This gate pulse and a signal from $N\overline{A}$ "coincidence" (neutrons and gammas) are fed into a coincidence circuit (K) whose output provides a "start" pulse for the time-to-height converter (to be referred to as THC). The signal N, from the neutron counter, could be either a neutron or a gamma; the anticounter A vetoes charged particles (for example, μ^- mesons) that pass through the target without stopping. The signal from $N\overline{A}$ is delayed by about 1.25 μsec, as shown in Fig. 3. The signals from $N\overline{A}$ that appear in this time interval give the background neutrons or gammas. The background rate is estimated by counting the number of neutrons or gammas in this range of channels.

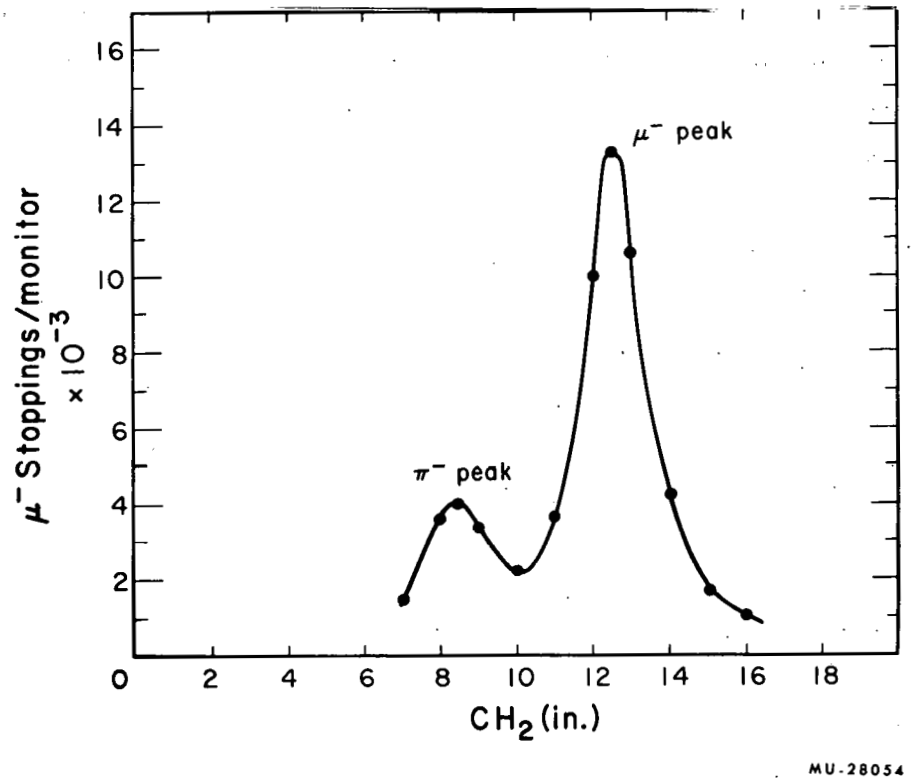

Fig. 2. Differential range curve of 200-MeV/c meson beam.

The "stop" pulse for the THC is fed from the output of the coincidence, $(S_3S_4\overline{AC})$ delayed by about 2.5 μsec. The delay is introduced because the THC is stopped by the μ^- stop signal, which appears earlier than the "start" signal (neutron or gamma). The coincidence output of K (start signal) already anticipates the stop signal. This ensures that the THC works only when there is a "start" signal followed by the "stop" signal. The THC produces a pulse proportional to the time delay between the neutron or gamma emission and muon stopping in the target. This pulse then feeds the Nuclear-Data 101 pulse-height analyzer which is gated by a neutron signal. This neutron signal comes from a pulse-shape discriminator which discriminates between a neutron and a gamma (to be described in Sec. C.). We should notice that the signal applied to the pulse-height analyzer for analysis could be either a neutron or a gamma. It is the neutron signal (that comes from the pulse-shape discriminator and gates the pulse-height analyzer) that tells the pulse-height analyzer whether it is a neutron or a gamma.

The time-to-height converter is an Eldorado Model TH 300 modified to cut off the rising ramp of the THC output pulse so that all the Pulses have the same rise time. The essential feature of this converter can be understood by considering the function of a pentode 6BN6. In the absence of any signal, the control grid of the pentode is held at approximately zero bias, but the suppressor grid is biased well below cutoff. The positive "start" gate is applied to the suppressor grid and is of sufficient amplitude to cause a plate current to flow in the tube. While the plate current is flowing, the plate voltage drops linearly with time, charging a capacitor between the plate and ground. The "stop" gate is applied to the control grid. The stop gate, being negative, cuts off the plate current in this tube and stops the linear charging of the plate capacitor. The capacitor then discharges until the start pulse starts its recharging again. The output pulse height is proportional to the time delay between the start and stop pulses.

The linearity of the THC was checked by simulating the coincidence output of $N\overline{A}$ from a pulser with a repetition rate of 10 kc. The output of the μ^- stop signal $(S_3S_4\overline{AC})$ was simulated by the S_3 scintillation

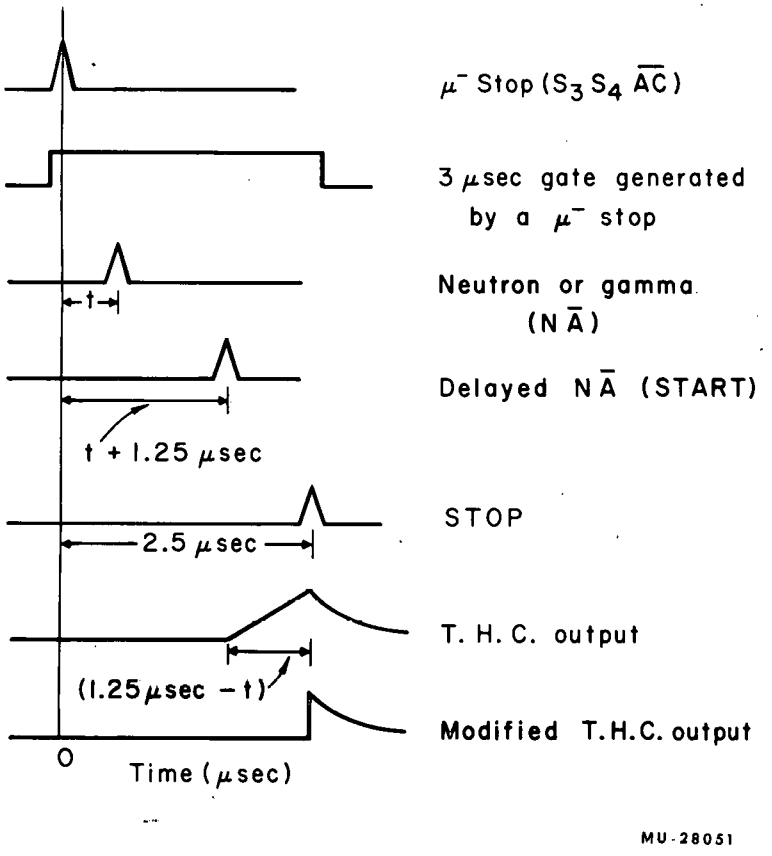

Fig. 3. Time relationship of different pulses in the electronic circuitry.

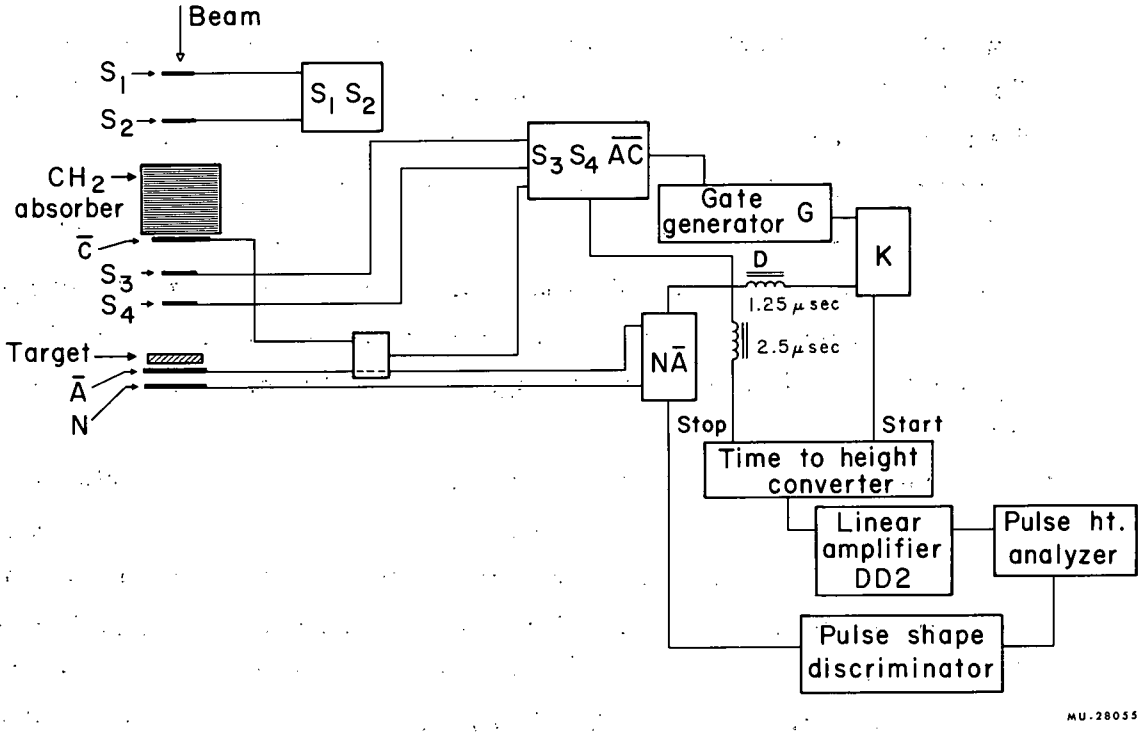

Fig. 4. Schematic diagram of electronics.

counter alone counting a Na^{24} source. The radioactive source provided stop pulses which occurred randomly in time. Because the time intervals between the occurrence of a start pulse and the following stop pulse are of random lengths, the spectrum displayed on the pulse-height analyzer (PHA) is a random-height spectrum and, for linear behavior of both the THC and PHA, should give equal probability of a pulse appearing in each channel. The data from a typical run are shown in Fig. 5. These data were fitted to a straight line $n_i = mi + n$ where n_i represents the number of counts in the ith channel, and i the channel number. The deviation from linearity is given by m/n. For this typical run, $m/n = (1.174 \pm 0.356) \times 10^{-4}$ and $n = 973 \pm 4.20$. While making this fit, we used only 210 channels out of the total 256. The first 30 and the last 16 channels were not taken into consideration, as these displayed some nonlinearity. This nonlinear region has not been used in the data analysis either.

The THC was calibrated by varying the delay, D (Fig. 4). Delay D was otherwise kept at 1.25 μsec. For each delay, a particular channel of the analyzer recorded the maximum number of counts. In the ideal case, only one channel should register counts corresponding to a particular delay. But the counts for one particular delay, in general, had a Gaussian distribution with a full width of less than two channels. The centroid of the channels was found. Each channel was weighted proprotionally to the number of counts in it. A typical calibration curve for the measured points is shown in Fig. 6. The calibration data are also given in Table II.

The time-calibration data were fitted to a straight line $y_i = ax_i + b$, where y represents the delay in nsec and x the channel number. The slope "a" gives the calibration time in nsec/channel. For the typical run shown in Fig. 6, a = 8.91 nsec/channel, and the standard deviation did not exceed 0.2 channel over the range of channels used.

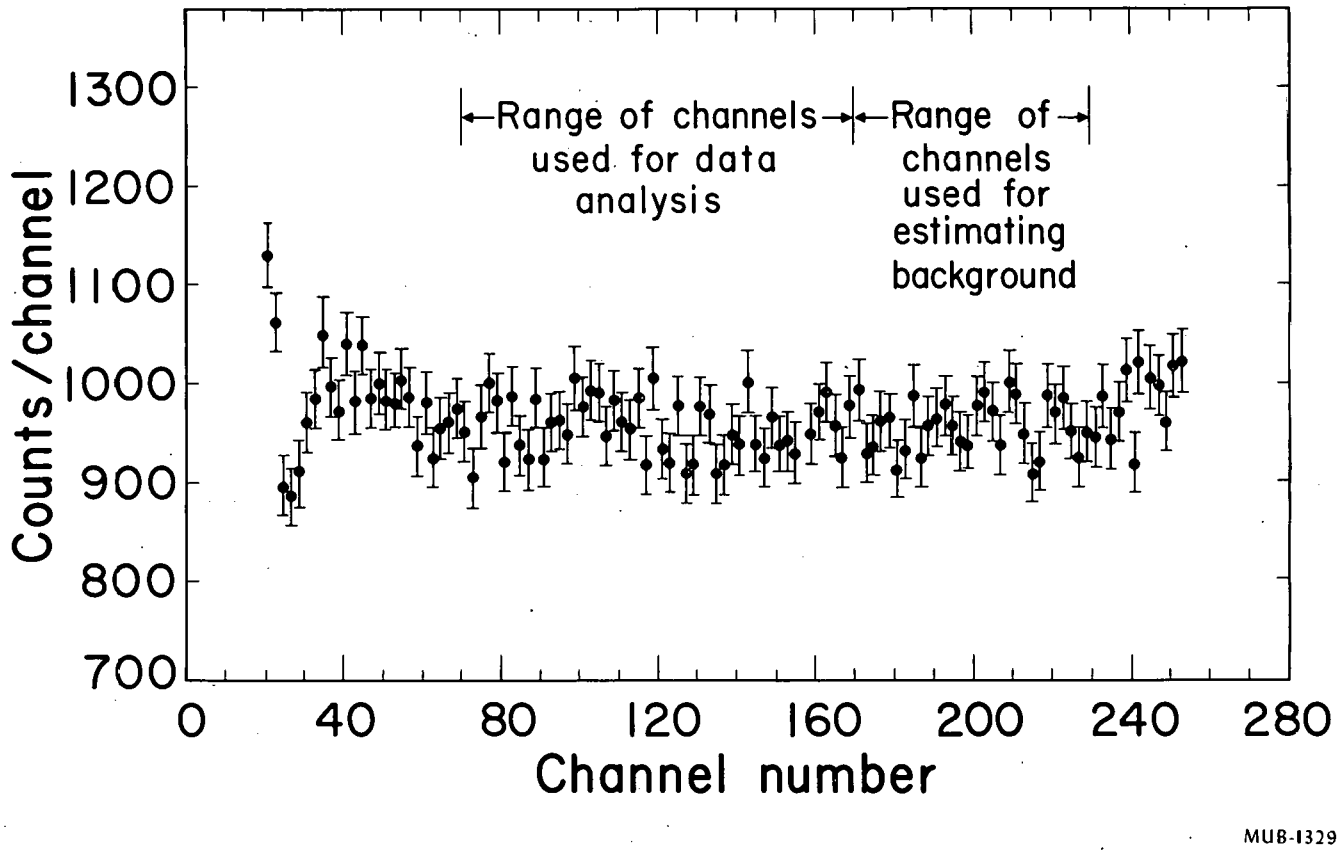

Fig. 5. Plot showing the linearity of time-to-height converter. A least-squares fit of the data to a straight line shows the linearity to be $(1.174 \pm 0.356) \times 10^{-4}$. Note that channel number 170 here corresponds to zero time channel in Figs. 8-20.

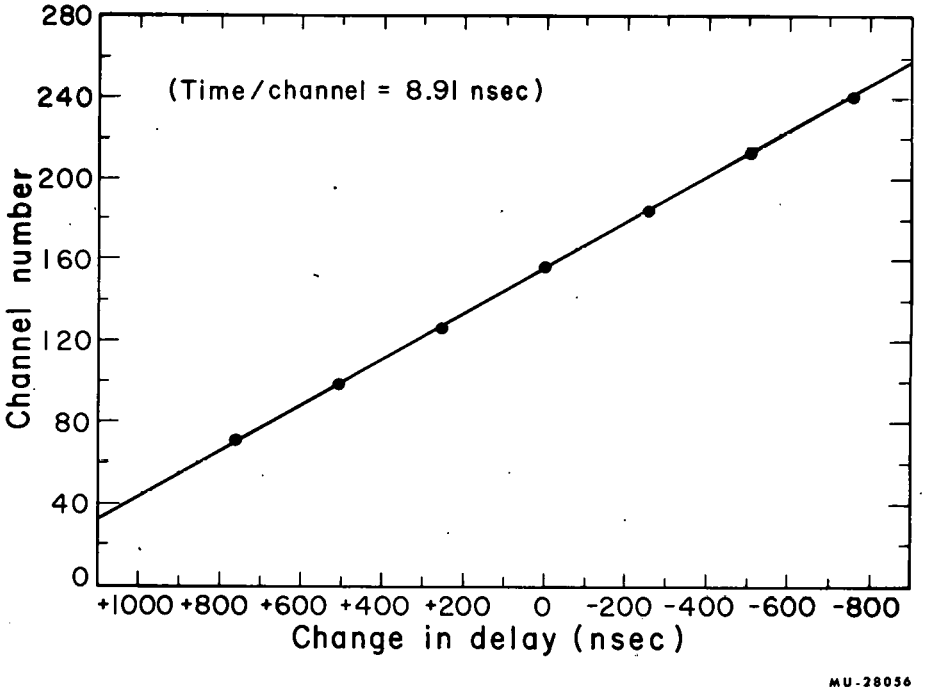

Fig. 6. Plot of the pulse-height analyzer channel number vs the spacing in time between "start" and "stop" pulses.

Table II. Typical time calibration data for the time-to-height converter.

Change in delay (nsec) Y_i	Channel number (from counts) X_i	Channel number (calculated from best fit)	Fraction of channel Δ_i
-757.1	241.06	241.23	+0.17
-501.6	212.84	212.69	-0.15
-254.8	185.17	185.12	-0.05
0	156.87	156.66	-0.21
+257.4	127.71	127.91	+0.20
+504.6	100.10	100.30	+0.20
+760.1	71.91	71.76	-0.15
$\chi^2 = \Sigma \Delta_i^2 = 0.201$		a = 8.95 nsec/channel	
variance = 0.201/5 = 0.040		b = 1402.53 nsec.	
standard deviation = 0.2			

The time delays were made by inserting calibrated RG 63-U cables into the circuit. The apparatus for calibrating these cables consists of two pulse generators. Each one of them produces a pulse whose time separation is adjustable and known. The time base for the measurement of the pulse separations is provided by a 1-Mc crystal-controlled oscillator. The pulse separation can be varied in definite time steps of 20 nsec each (50 Mc). We also have a vernier which permits adjustment of one of the 20-nsec steps to 0.1 nsec accuracy to cover the range of in-between steps. The vernier is essentially an adjustable phase-shifting network. In practice, one first adjusts the timing of the two pulses to be in coincidence. Then the length of unknown cable to be measured is inserted in series with one of the pulses. The two pulses are now no longer in coincidence, as one pulse must travel through the length of unknown cable. However, the pulse that is traveling through the unknown cable can be started earlier in time to

bring the two pulses into coincidence again. The amount the pulse had to be advanced in time to produce coincidence again is known and hence the length of the cable can be measured. For shaped pulses of the type used in this experiment, our apparatus was used to measure the delay of two 2-μsec cables, separately first and then in series. The two measurements agreed within 1 nsec.*

C. Neutron Counter and Pulse-Shape Discriminator

To detect neutrons in the presence of gamma rays, we used a pulse-shape discriminator with the neutron scintillation counter. This discriminator is essential, since the rate of emission of gamma rays is comparable with that of neutrons.

The neutron counter consists of a 5-in. o.d. by 1-in.-thick glass container filled with liquid scintillator. The liquid scintillator used was Nuclear Enterprise 212. The glass container was attached to a RCA 7046 photomultiplier tube by means of a lucite pipe. The scintillator was flushed continuously with dry argon gas to remove oxygen, as oxygen in liquid scintillators destroys the pulse-shape discrimination properties.

The principle of pulse-shape discrimination can be understood as follows: Neutrons produce recoil protons and γ rays produce Compton electrons. The scintillation pulse shapes produced by these secondary particles are different. The scintillation-light output can be described by a combination of exponentials of two different time constants. The amplitude ratios of these fast and slow output components are different for different kinds of particles. This fact is utilized in discriminating between different particles.

Several types of circuits have been developed as pulse-shape discriminators.[22,23] In the present pulse-shape discriminator, the discrimination is carried out by a circuit connected to the last dynode of the photomultiplier. The circuit is shown in Fig. 7. The earlier

* The author would like to thank Mr. Cordon Kerns who designed the above apparatus and performed the cable measurements.

part of the pulse (fast component) drives a Q6100 diode which presents a low impedance to the incoming pulse. An RC circuit (time constant 0.5 μsec) then produces an output pulse proportional to the light in the fast component. The later part of the pulse (slow component) goes through a 1-kΩ resistor and then through an RC circuit (time constant 0.5 μsec) which produces an output pulse proportional to the light in the slow component. The larger of the two pulses is attenuated and inverted. The pulses are then mixed and the attenuator is adjusted in such a way that the output pulse is negative for γ rays and positive for neutrons.

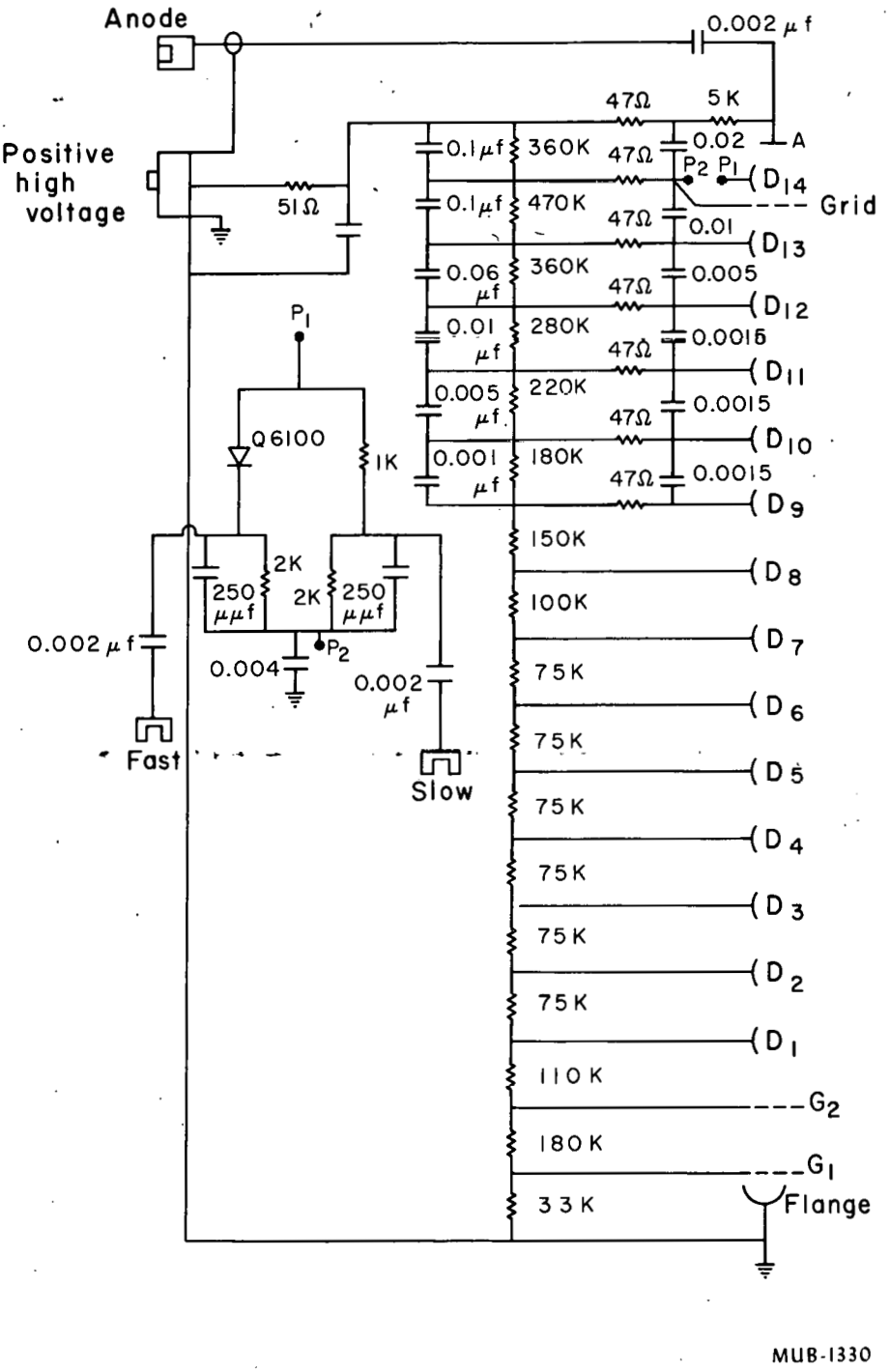

Fig. 7. Photomultiplier tube base for RCA 7046 tube. The points P_1 and P_2, on the pulse shape discriminator that separates out the fast and slow parts of neutron and gamma pulses, is connected to the last dynode (14).

IV. EXPERIMENTAL PROCEDURE

The relative atomic-capture probability of μ^- mesons was measured by finding the lifetime curve that, for a single element, is furnished by an exponential whose intercept gives the rate of emission of capture products and the inverse of slope, the lifetime. In the case of a binary compound, the lifetime curve is composed of two exponentials corresponding to the different lifetimes of the μ^- meson in the two elements of a compound. This composite curve can then be decomposed into two curves, each of which corresponds to a particular element. The intercepts at zero time for each curve can then be used to find the relative number of μ^- mesons stopping in the mesic K shell of different nuclear species in the compound target.

Several runs for each element and compound target were taken. Each target was run for an hour at a time or sometimes more. To find the relative atomic-capture probability, we have compared the relative captures in the constituents of the compound with those in the separate elements. Because this method was used, we ran the compound and the separate elements consecutively to minimize the effects of long-term time drifts. In this way about 3000 neutrons were collected in an hour for 10^5 μ^--meson stoppings for a target of thickness 5.0 g/cm^2. Each target was run at least twice.

The counting rate of the neutron counter was also checked at regular intervals by using a PuBe source in some fixed position and recording the counting rate. The counting rate did not change by more than 1%. This was done to ensure that the overall sensitivity of the neutron counter remained constant.

V. ANALYSIS OF DATA

A. General Outline

The data recorded during the various runs were the number of μ^--meson stoppings and the time distribution of neutrons emitted after the stoppings, presumably caused by nuclear capture of μ^- mesons from the K shells. The rate of disappearance of μ^- mesons from the mesic atoms's K orbit can be written as

$$\frac{dN}{dt} = -\Lambda N , \tag{8}$$

or

$$N = N_0(Z)e^{-\Lambda t} , \quad \text{and} \quad \Lambda = \Lambda_d + \Lambda_c, \tag{9}$$

where $N_0(Z)$ is the number of muons bound to the K orbit of an element of atomic number Z at t = 0. This is the same as the total number of mesons stopping. The Λ is the total disappearance rate. The Λ_d and Λ_c are the muon-decay and nuclear-capture rates, respectively.

The observed neutron time distribution Y(t) is proportional to $\frac{dN}{dt}$ and the detection efficiency E of the neutron detector. Therefore we can write

$$Y(t) = E' N_0 \Lambda_c e^{-\Lambda t} + B, \tag{10}$$

where B is the background rate, and E' is the detection efficiency of the detector for neutrons from the element. For a binary compound,

$$Y(t) = E_1 C_1 N_0 \Lambda_c(1) e^{-\Lambda(1)t} + E_2 C_2 N_0 \Lambda_c(2) e^{-\Lambda(2)t} + B, \tag{11}$$

where E is the detection efficiency for the constituent element in the compound, and C_1 and C_2 are the atomic-capture probabilities, and their sum should be unity.

The subscripts 1 and 2 identify the two elements of the compound. The detection efficiency includes the effects caused by the different neutron energy spectra for the different elements, the neutron multiplicity, and the attenuation of neutrons in the target.

B. Lifetime Measurements

The neutron time-distribution data for an element was least-squares-fitted to Eq. (10) with the help of an IBM 704 program known as FRENIC. The program makes a least-squares fit by a process of iteration.

To find the lifetime of μ^- mesons in a certain element, we put in the estimates of the lifetime and the intercept (which is the rate of emission of neutrons at zero time). The background parameter was kept constant. Then the program was used to calculate the intercept at zero time and to calculate the lifetime. The goodness of fit of data was tested by applying a χ^2 test. In all cases the $P(\chi^2)$ was between 0.10 and 0.90. The $P(\chi^2)$ is obtained from the table of χ^2 probabilities for a given number of degrees of freedom. In our case the numbers of degrees of freedom were larger than are given in standard tables. In such cases, $P(\chi^2)$ was calculated by using a method given in Ref. 27.

Several runs for each elemental target were taken. The weighted average of these measurements was found. Then a χ^2 fit of these measured values to the average was made. For all those cases in which the variance was greater than unity, the error on the average lifetime was multiplied by the square root of the variance. This procedure allows for nonstatistical fluctuations in the data. The errors thus quoted take into consideration both counting statistics and reproducibility. The results are given in Appendix B.

C. Z Law Measurements

The Z law data were analyzed as follows: The neutron time-distribution data from a compound target were least-squares-fitted to Eq. (11), with the help of the FRENIC program. To carry out the analysis we inserted the known background, the known values of the lifetimes, and the estimates of the intercepts at zero time. Then the parameters for the background and the lifetimes were held constant, while the program was used to calculate those the intercepts designated in terms of the symbols of Eq. (11) as $E_1 C_1 N_0 \Lambda_c(1)$ and $E_2 C_2 N_0 \Lambda_c(2)$.

To find C_1 and C_2, we have to know $E_1' N_0 \Lambda_c(1)$ and $E_2' N_0 \Lambda_c(2)$ for the separate elements forming the compound. To find $E_1' N_0 \Lambda_c(1)$ and $E_2' N_0 \Lambda_c(2)$, we fitted the data for the elements to Eq. (10), again with the help of FRENIC. This time the parameters for background and the lifetimes were held constant. The program was used to calculate out the intercepts $E_1' N_0 \Lambda_c(1)$ and $E_2' N_0 \Lambda_c(2)$. These intercepts were corrected for the effects included in the detection efficiency E' and E.

The probability C_1 for atomic capture of μ^- mesons in one of the constituents in the compound was obtained by dividing the intercept for this constituent by that for the separate element. Similarly, the atomic-capture probability C_2 of the other constituent in the compound was obtained. The ratio C_1/C_2 gives the relative atomic-capture probability of μ^- mesons in the constituents of the compound .

The data for the sulfide compounds and the metallic solution CuAu were analyzed along the lines mentioned above. From the results given in Table IV (Sec. VII) we notice that the sum of atomic-capture probabilities for compounds adds up to nearly unity, while in the case of CuS, it is 0.78, which is far from unity. Our suspicions arose about the purity of the targets. Therefore, we had all the targets chemically analyzed.

The chemical composition of the CuS and PbS samples was found to be:

	In CuS		In PbS
CuS	65.82%	PbS	90.76%
$CuSO_4$	19.46%	$PbSO_4$	8.24%
H_2O	11.03%		

$\frac{\text{No. of oxygen atoms}}{\text{No. of copper atoms}} = 1.364$ $\qquad$ $\frac{\text{No. of oxygen atoms}}{\text{No. of lead atoms}} = 0.28$

All the other targets were found to be 99.8% pure. The target materials used were presumed to be reagent quality, so we do not know the cause of impurities in these targets.

To estimate the correction for the fraction of μ^--meson atomic captures in oxygen in copper sulfide, we first found the proportion of oxygen atoms to atoms of copper in the compound on the basis of the above chemical analysis. This ratio was found to be 1.364. From our experimental result for CuO (Sec. VII, Table V), we know that the ratio is $C_O/C_{Cu} = 0.163$, where C is the atomic-capture probability. This is based on the fact that the ratio of oxygen to copper atoms in the compound CuO is unity. But in our CuS target, it is 1.364. Therefore, multiplying 1.364 by 0.163 we estimate the ratio of captures in oxygen to that in Cu in our CuS target. This number is 0.222. From the experimental result for CuS, we know that about 51% of the captures take place in Cu. So, multiplying 0.51 by 0.222 gives about 0.11, which is approximately the captures in oxygen. This simple argument accounts for about 11% of the missing μ^--meson captures. The effect of hydrogen, if any, is ignored. Applying this correction brings the sum of atomic-capture probability from 0.76 to about 0.87. To bring the sum closer to unity, we have to account for about 13% more μ^- mesons. The results of Sens et al. indicate that the captures in oxygen are enhanced by a factor of two in the case of light oxide compounds. This is an experimental finding that has received no explanation. Using this fact, we can account for another 11% of the missing μ^- mesons.

Similarly, it was found that for PbS about 5% of the μ^- captures take place in oxygen, owing to the presence of sulfate ions. When this correction was applied, the sum of atomic-capture probabilities changed from 0.89 to 0.94.

The data analysis for oxide compounds needs a separate consideration. We tried to separate the yield of neutrons from oxygen but it was found to be statistically insignificant. This is probably due to the following reasons. First, since oxygen has an atomic number of eight, only about 25% of the μ^- mesons reaching the mesic K shell in oxygen are captured by the nucleus. Second, the yield from oxygen was distributed over a much larger number of channels than from the heavier element. For example, consider the case of CuO. The mean lifetime of the μ^- meson in oxygen is about ten times that in Cu (163 nsec). The number of channels used in data analysis was about three mean lifetimes in Cu. This range of channels is equivalent to only three-tenths of the mean lifetime in oxygen. Third, the low neutron multiplicity in oxygen also reduces the neutron yield. Therefore, it is reasonable that we did not observe any yield of neutrons from oxygen. Since the sum of atomic-capture probabilities should equal unity, we obtained the atomic-capture probability in oxygen by subtracting from unity the atomic-capture probability of the element in the oxide compound.

The data for AgLi were analyzed in the same way as was done for oxides. Examples of the lifetime distribution of neutrons from μ^--meson captures in different compounds and elements are shown in Figs. 8 through 20. The constituent elements in the compounds (sulfides and CuAu) have been peeled off as shown.

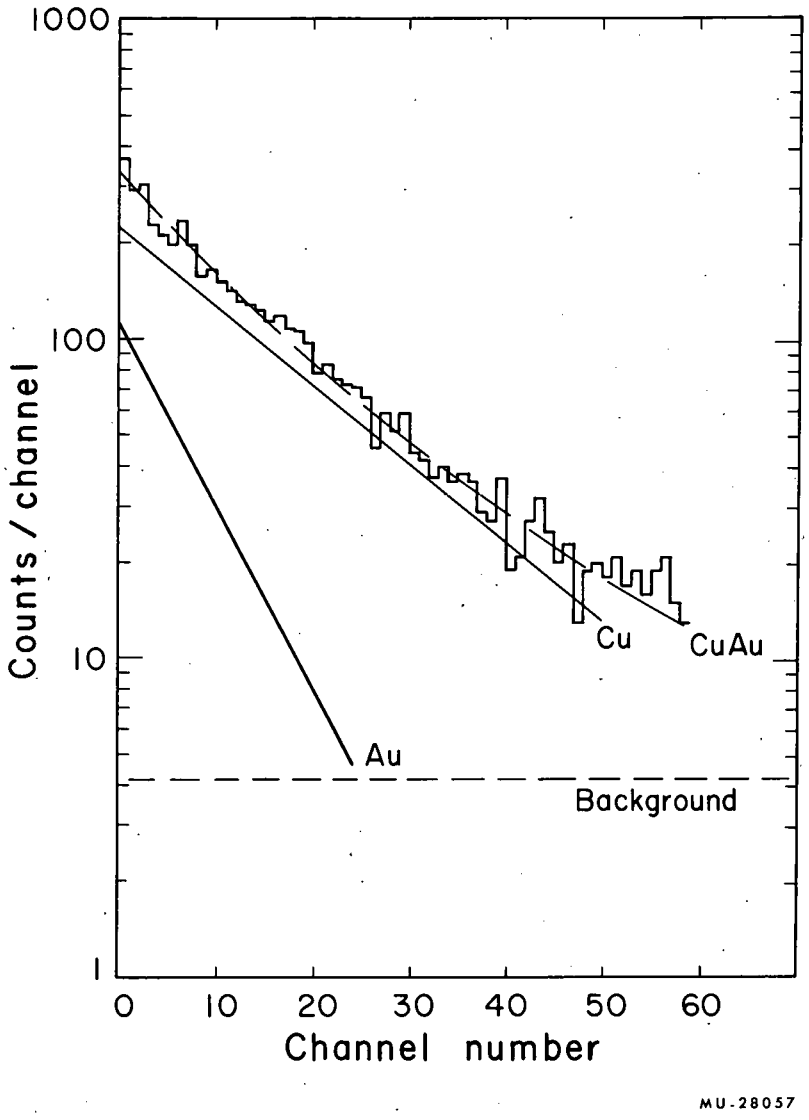

Fig. 8. Lifetime distribution of μ^- mesons in CuAu (background included). The curve has been peeled off for μ^- meson lifetime in the constituent elements in the compound (background subtracted). The dotted line indicates the background. $P(\chi^2) = 0.705$.

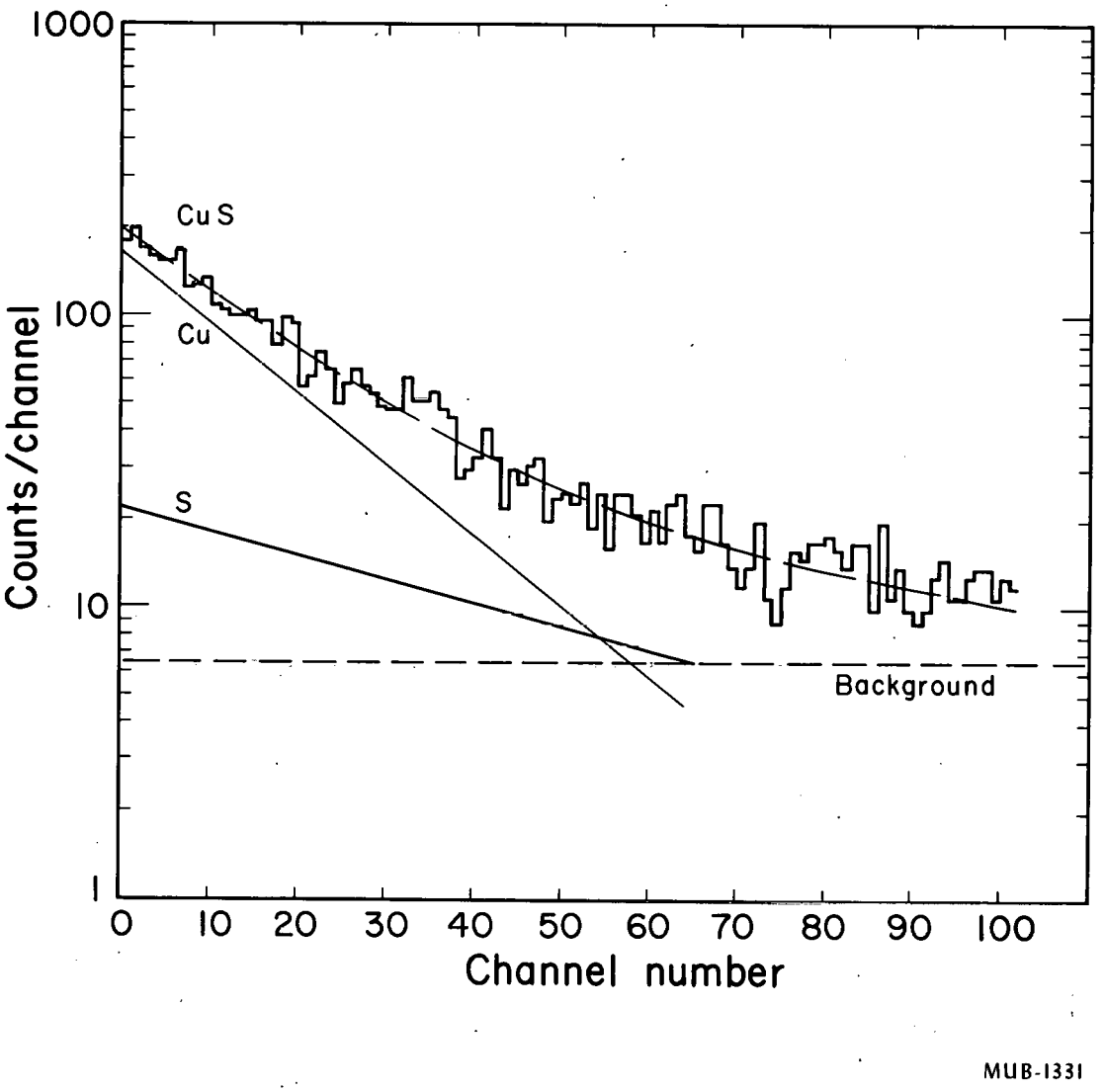

Fig. 9. Lifetime distribution of μ^- mesons in CuS (background included). The curve has been peeled off for μ^- meson lifetime in the constituent elements in the compound (background subtracted). The dotted line indicates the background. $P(\chi^2) = 0.755$

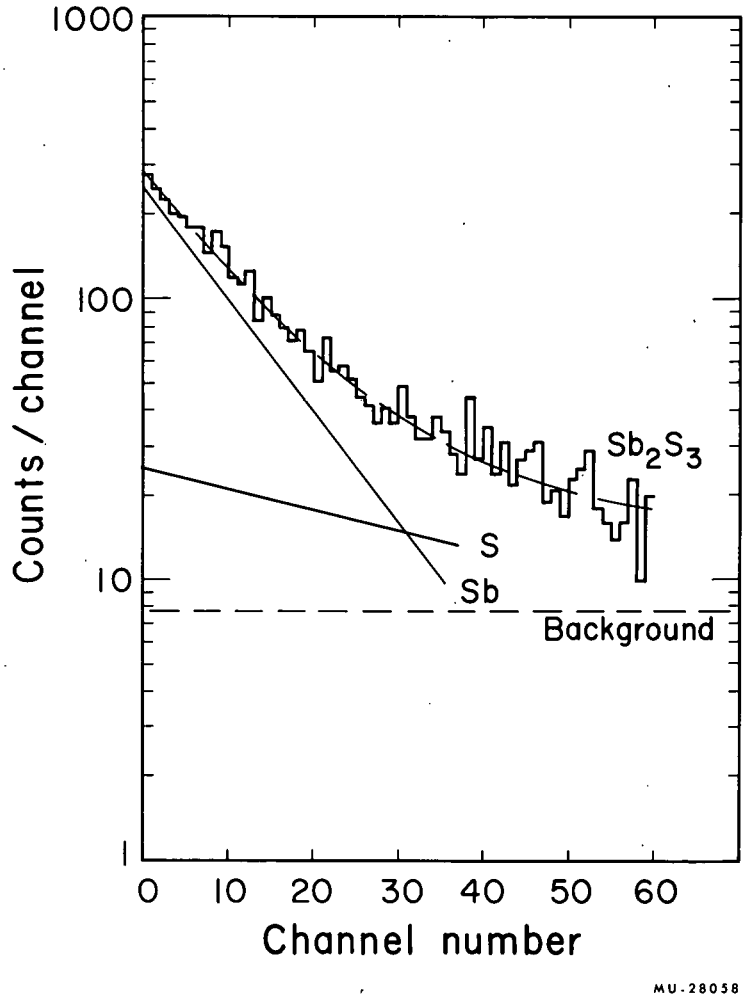

Fig. 10. Lifetime distribution of μ^- mesons in Sb_2S_3 (background included). The curve has been peeled off for μ^- meson lifetime in the constituent elements in the compound (background subtracted). The dotted line indicates the background. $P(\chi^2) = 0.343$.

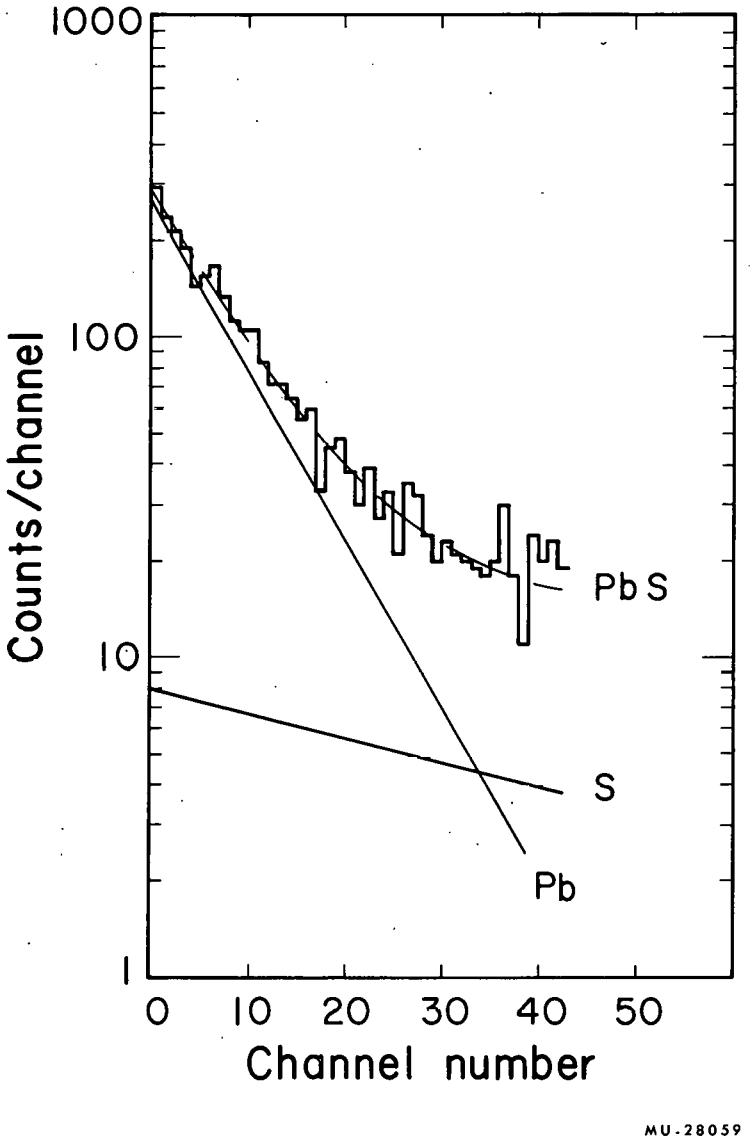

Fig. 11. Lifetime distribution of μ^- mesons in PbS (background included). The curve has been peeled off for μ^- meson lifetime in the constituent elements in the compound (background subtracted). The dotted line indicates the background. $P(\chi^2) = 0.274$.

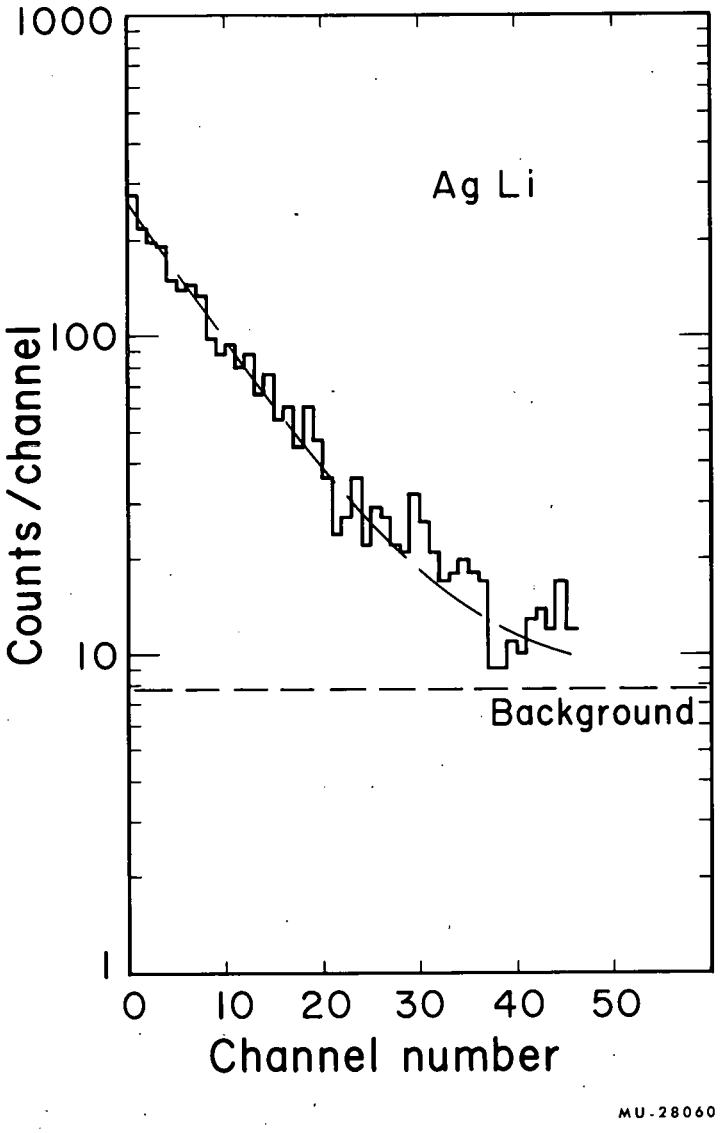

Fig. 12. Lifetime distribution of μ^- mesons in AgLi (background included). The dotted line indicates the background. $P(\chi^2) = 0.283$.

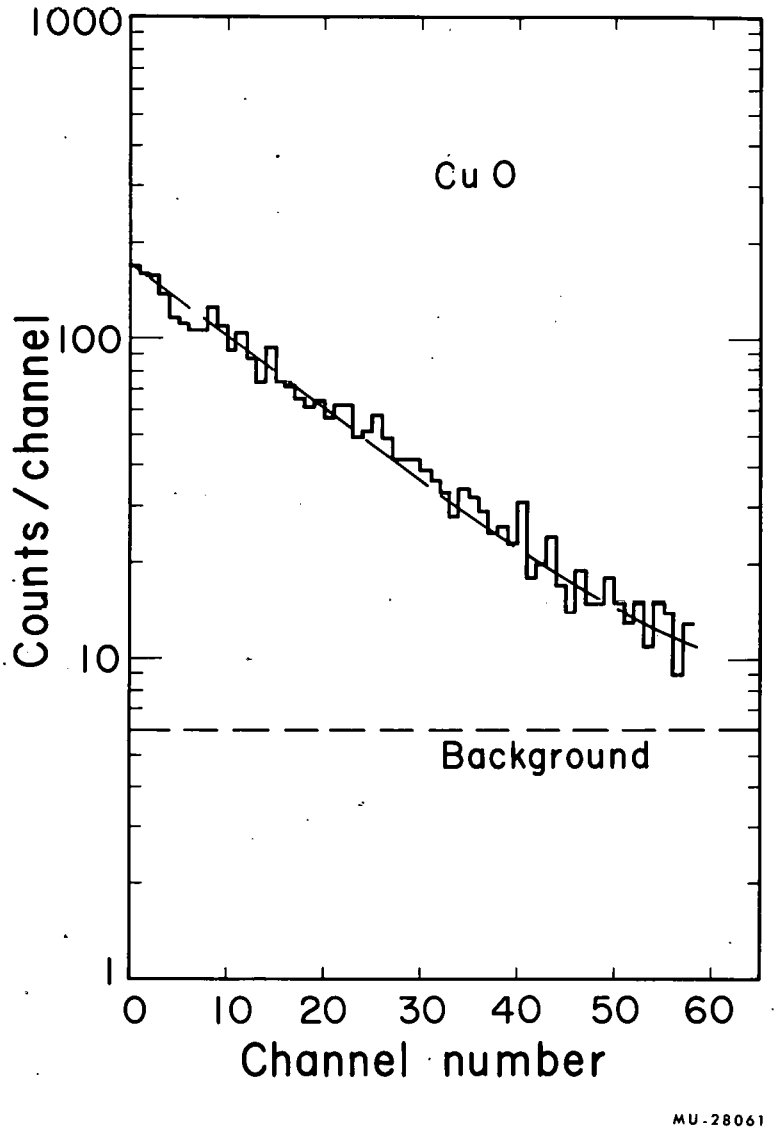

Fig. 13. Lifetime distribution of μ^- mesons in CuO (background included). The dotted line indicates the background. $P(\chi^2) = 0.391$.

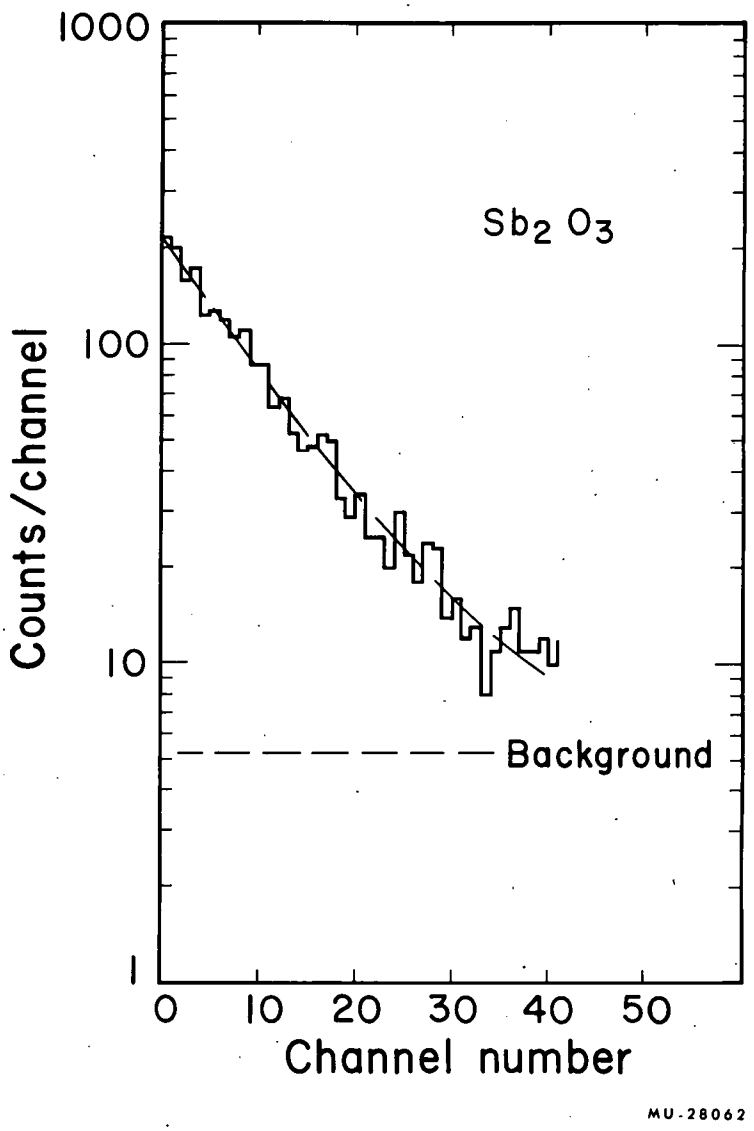

Fig. 14. Lifetime distribution of μ^- mesons in Sb_2O_3 (background included). The dotted line indicates the background. P (χ^2) = 0.444.

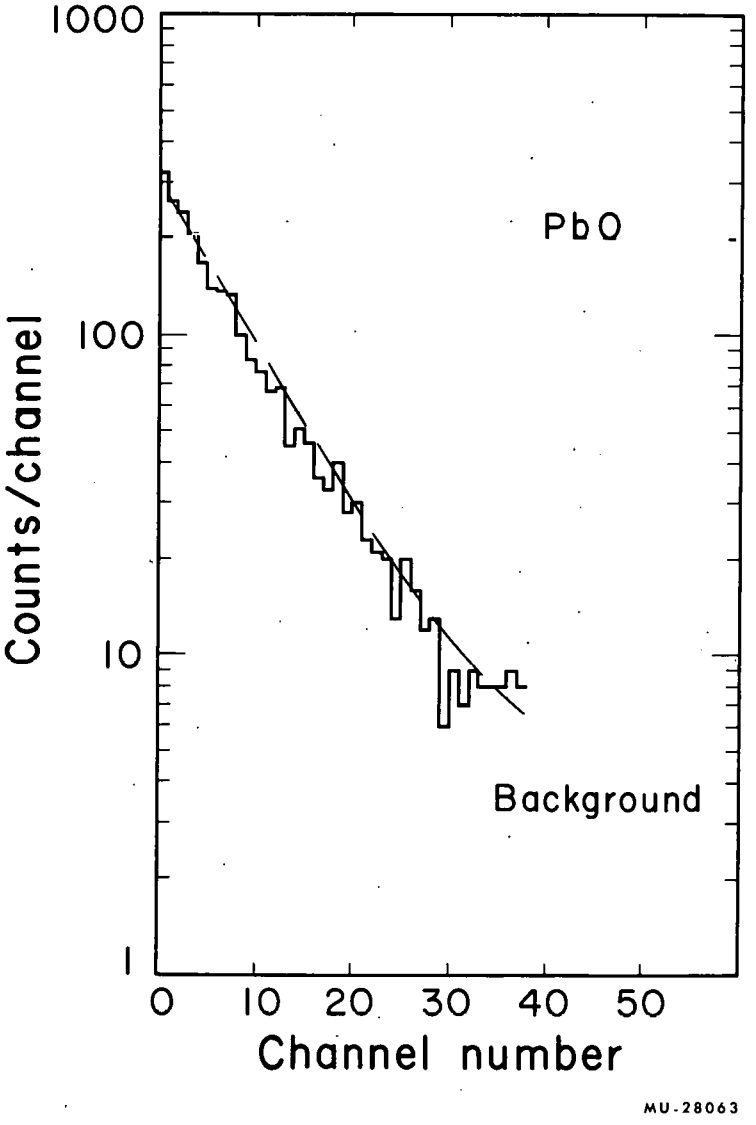

Fig. 15. Lifetime distribution of μ^- mesons in PbO (background included). The dotted line indicates the background. $P(\chi^2) = 0.903$.

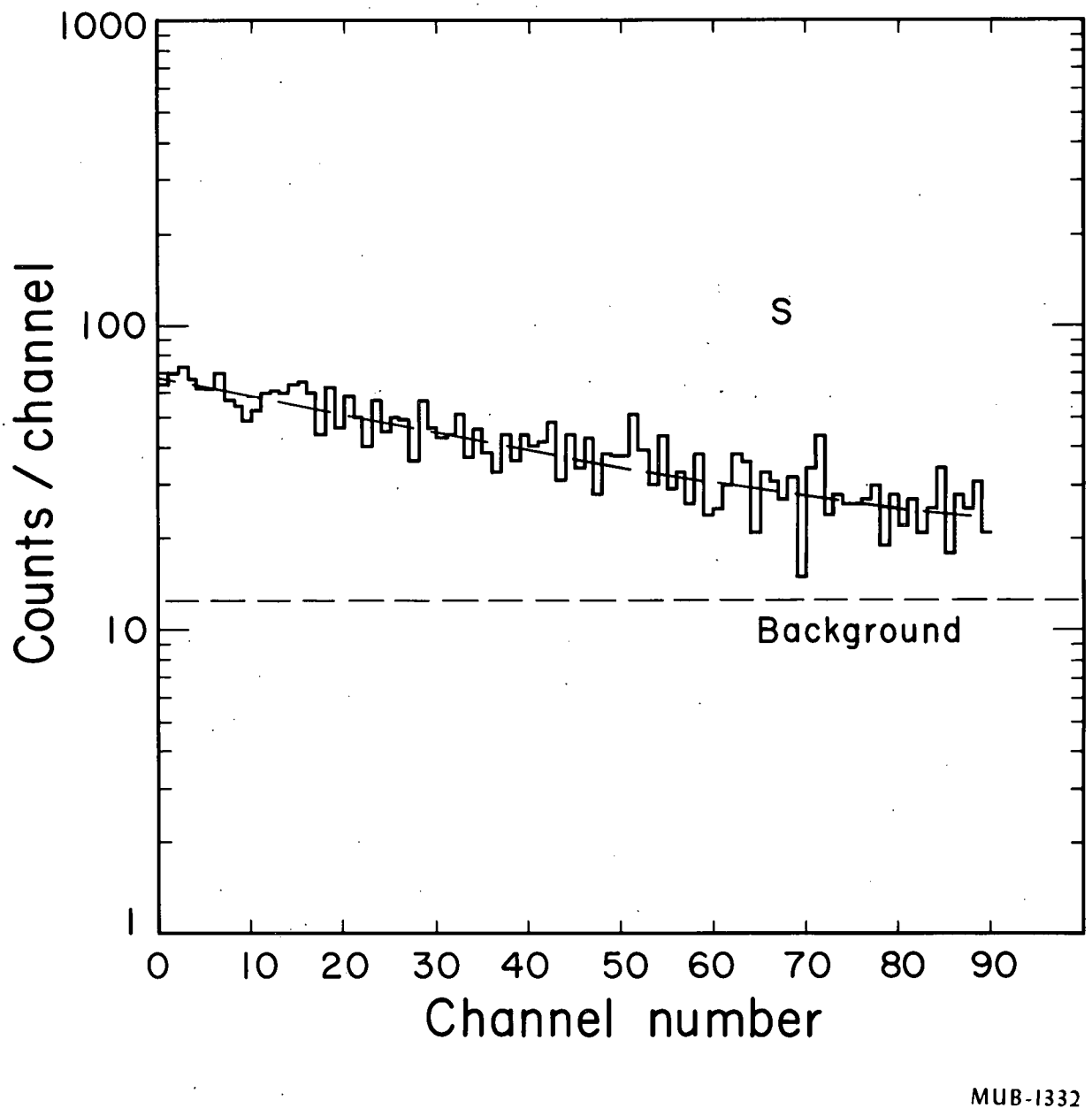

Fig. 16. Lifetime distribution of μ^- mesons in Sulfur (background included). The dotted line indicates the background. $P(\chi^2) = 0.352$.

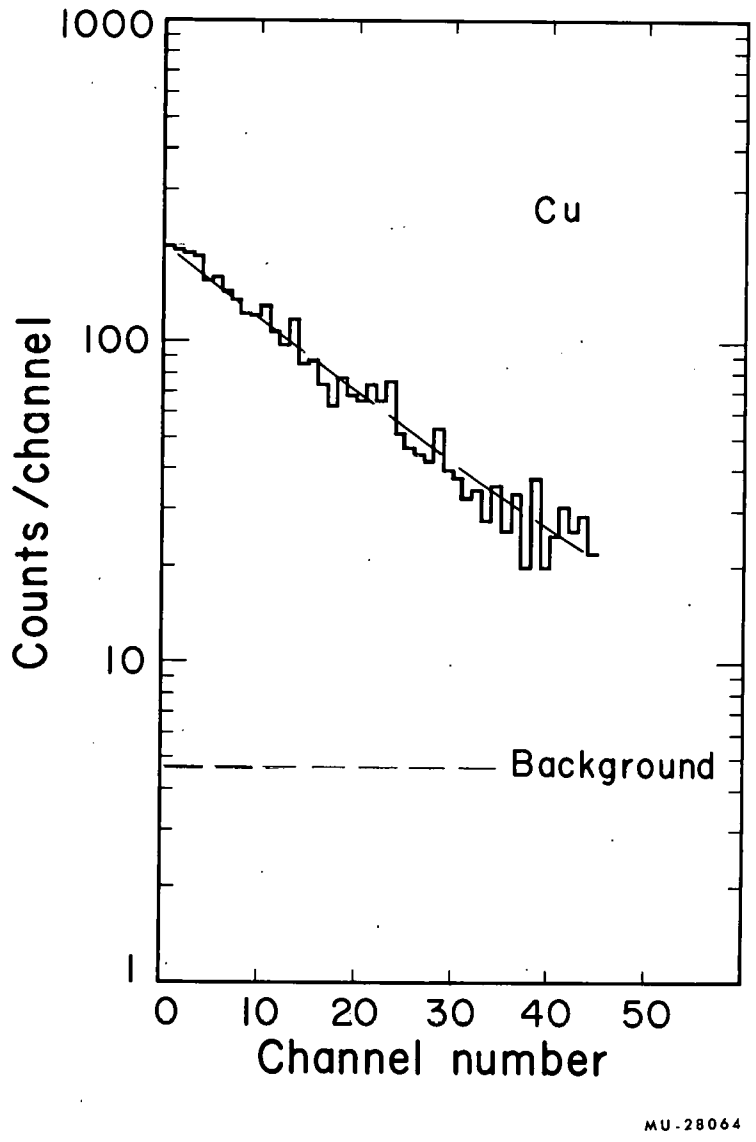

Fig. 17. Lifetime distribution of μ^- mesons in Cu (background included). The dotted line indicates the background. $P(\chi^2) = 0.597$.

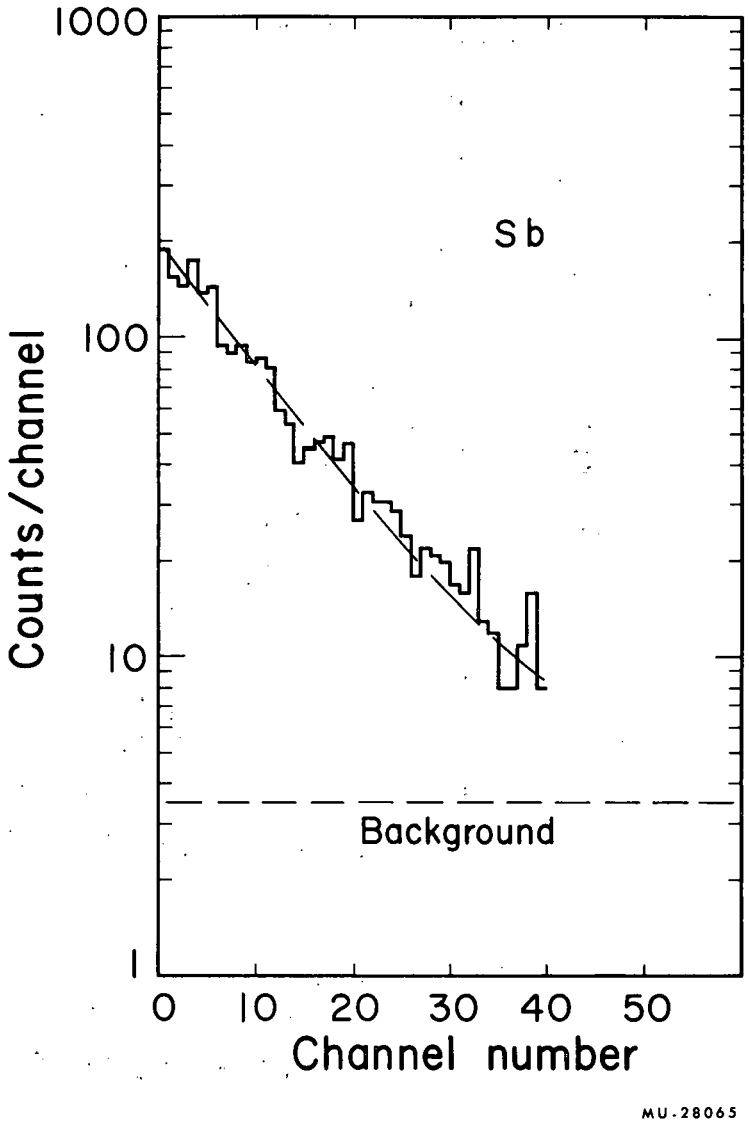

Fig. 18. Lifetime distribution of μ^- mesons in Sb (background included). The dotted line indicates the background. $P(\chi^2) = 0.348$.

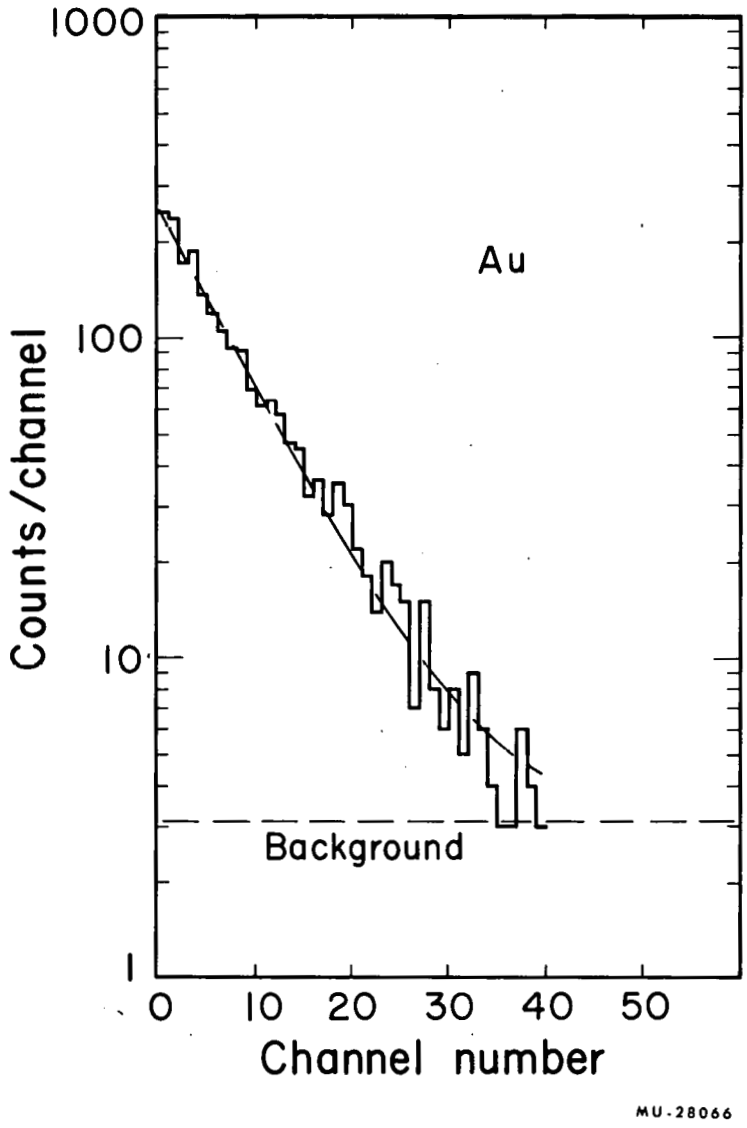

Fig. 19. Lifetime distribution of μ^- mesons in Au (background included). The dotted line indicates the background. $P(\chi^2) = 0.773$.

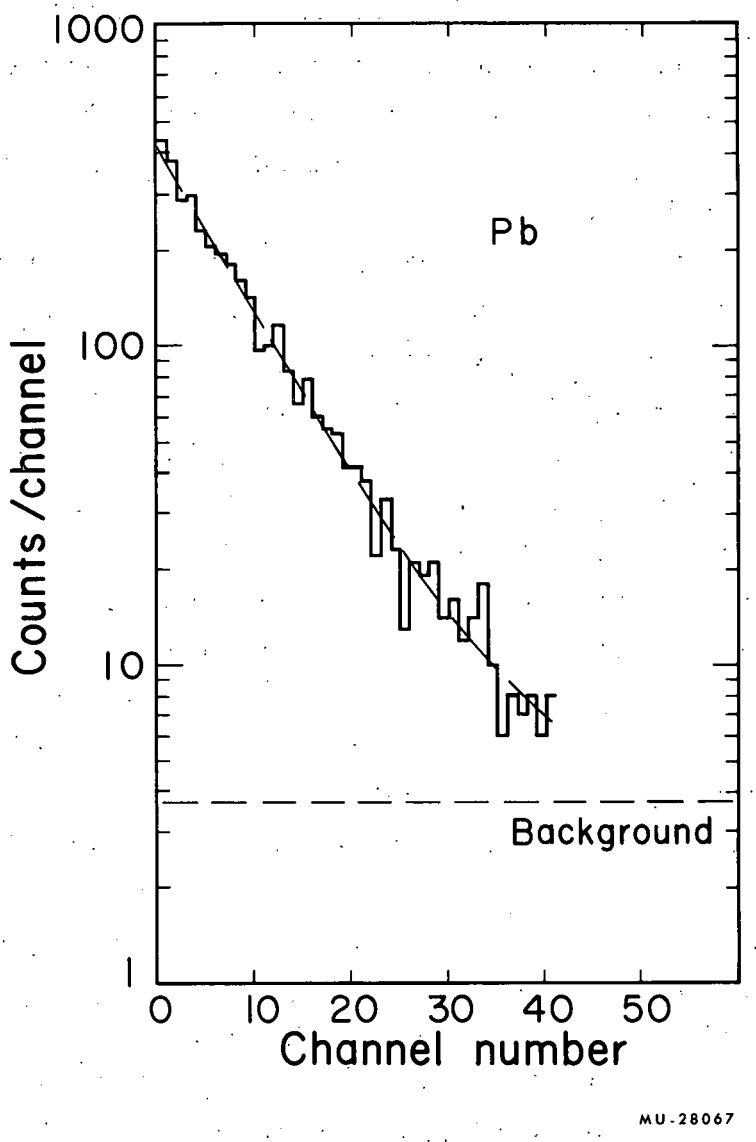

Fig. 20. Lifetime distribution of μ^- mesons in Pb (background included). The dotted line indicates the background. $P(\chi^2) = 0.311$

VI. CORRECTIONS

A. Geometric Correction

An effort was made to have the compound and elemental targets of the same density and thickness. Some of the compound targets were available in powder form; therefore, to match the low density of these targets, the metallic targets were also made in powder form. In spite of this, we had slightly different thicknesses for the targets. Different solid angles were subtended at the neutron counter by different sections of the target. A correction was applied in the following way.

In a separate experiment, the muons were stopped in an Au target approx 0.15 in. thick. This Au target was thin compared with the other targets used in the experiment. At first the target was placed touching the anti-counter A, which was against the neutron counter N. The number of neutrons detected per muon stopping in the target in this position was then recorded by the neutron counter. The Au piece was then moved to different positions at distances X_i with respect to the neutron counter. The number of neutrons detected per muon stopping was recorded for each target position. The numbers of neutrons per muon stopping in different positions were normalized to the number measured when the Au piece was touching the anti-counter. Let us call it $g(X_i)$. This function, which gives the solid-angle effect, is plotted on Fig. 21. To find the geometric correction, a numerical integration was made over the thickness of the target.

Suppose $M\Delta X$ is the muon stoppings in the target thickness ΔX. If $g(X)$ is the corresponding solid-angle effect as found from the curve, then the geometric correction to be applied is

$$G = \frac{\sum_i M(X_i)\,\Delta X_i\, g(X_i)}{\sum_i M(X_i)\,\Delta X_i}$$

The summation extends over the whole target thickness. The effect of neutron attenuation has been shown in Sec. VI. B. This was

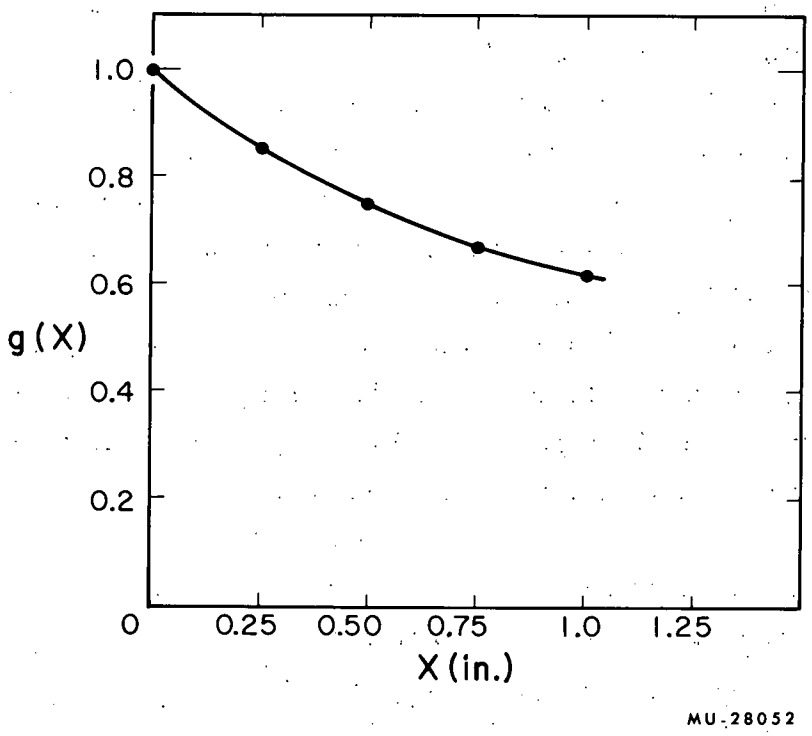

Fig. 21. Curve showing the relative solid-angle effect with respect to Au.

done to show separately the effects of geometry and neutron attenuation.

The $M(X_i)$ was found from the differential range curve. Since the differential range information was obtained with the CH_2 absorber increased by 1/4-in. increments, a convenient differential target thickness to use for this numerical integration was the thickness equivalent in stopping power to 1/4 in. of CH_2. This differential thickness for most targets was less then 1/8 in.

If Y_i represents the thickness equivalent to CH_2, then X_i is to be replaced by Y_i in the above expression for G.

To illustrate the above, we take a specific example of Pb target. The μ^- stoppings per monitor for this target are known from experiment. Using this and the integral range curve (Fig. 22), we can find the thickness of Pb equivalent to CH_2. This equivalent target thickness (Y_i) is then divided into different pieces of 1/4-in. thickness. Using the differential range curve (Fig. 23), we can find the muons stoppings in each 1/4 in. of CH_2. This gives $M(Y_i)$. Therefore, G can be calculated, since other quantities are also known.

The relative geometric factors of different compound targets with respect to the elemental targets are:

CuS/Cu (powder) = 1.00

CuS/S_I = 1.11

CuS/S_{II} = 0.990

PbS/Pb (powder) = 0.88

PbS/S_I = 1.05

PbS/S_{II} = 0.940

Sb_2S_3/Sb^{thin} = 0.88

Sb_2S_3/Sb^{thick} = 0.96

Sb_2S_3/S_I = 1.11

Sb_2S_3/S_{II} = 0.99

CuO/Cu (powder) = 0.95

$Sb_2O_3{}^{thin}/Sb^{thin}$ = 0.97

$Sb_2O_3{}^{thick}/Sb^{thick}$ = 0.92

$Sb_2O_3{}^{thin}/Sb^{thick}$ = 1.06

$Sb_2O_3{}^{thick}/Sb^{thin}$ = 0.84

PbO/Pb (powder) = 0.98

$CuAu/Cu$ (solid) = 0.97

$CuAu/Au$ = 0.88

$AgLi/Ag$ = 0.97

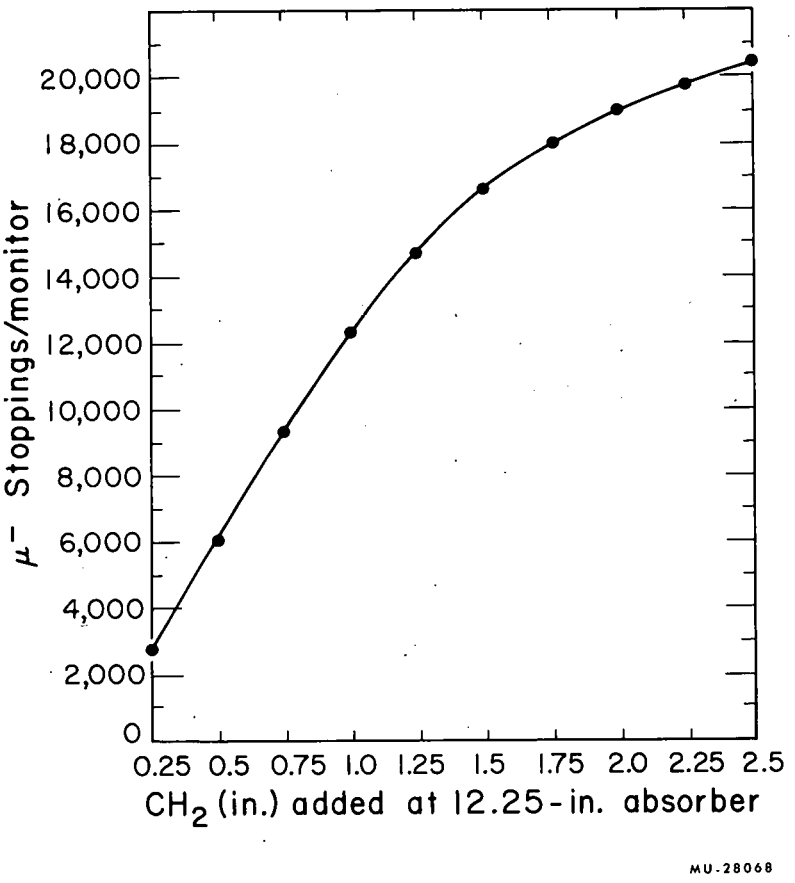

Fig. 22. Integral stopping rate in CH_2.

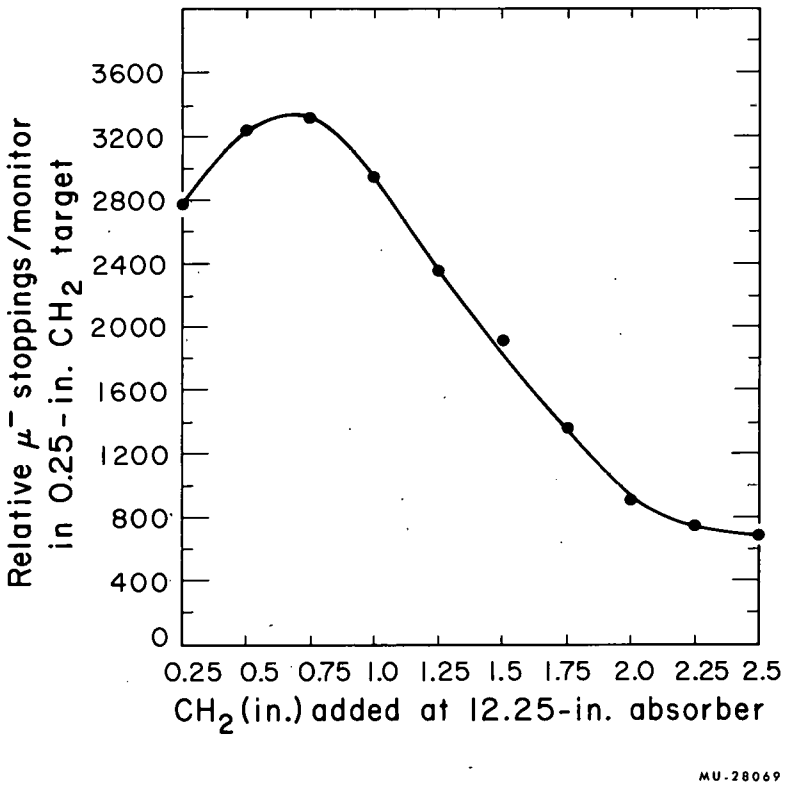

Fig. 23. Differential stopping rate in 1/4-in. CH_2.

The S_I and S_{II} are two pressed-sulfur targets of different densities. Among the oxides, the Sb_2O_3 targets were of two different densities. We varied the densities to see if the larger amount of oxygen in the target attenuated the neutrons more and thus affected the neutron emission. The Sb_2O_3 was chosen because the stoichometric ratio in it was higher than in our other oxide compounds. The neutrons emitted per μ^--meson stopping for both the thin and thick Sb_2O_3 targets were identical within statistical errors. This indicated that the presence of oxygen caused no special attenuation problem, which is also supported by the neutron-attenuation measurements for these targets made with a mock fission source. The neutron attenuation per g/cm^2 for both the thin and thick targets was the same (see Table III, Sec. VI. B). The results given in Tables IV and V (Sec. VII) are the average of the results for the two targets.

B. Neutron Attenuation in Targets

The neutrons from μ^--meson capture are produced throughout the volume of the target. These neutrons undergo different amounts of attenuation depending upon their places of origin. This attenuation results in decreasing the yield of the neutrons.

To correct for this neutron attenuation effect in different targets we performed a separate experiment with a mock-fission neutron source. It was assumed that the neutron spectrum from this source resembles an evaporation spectrum with respect to both average energy and shape. This experiment, however, gave only an upper limit to the attenuation effect, since the neutron source was at the surface of the target farthest from the neutron counter. But the neutrons resulting from μ^- meson capture are nonlocalized in the target. To find the effect of nonlocalization, it is necessary to consider the distribution of the neutrons inside the target as well as the neutron attenuation in different sections of the target. It was assumed that the distribution of neutrons in each section of the target was proportional to the distribution of the μ^--meson beam inside the target.

First, the attenuation was measured with the source position at the surface of the target. This was then used to calculate the total cross section σ from the formula $P/P_0 = 1 - e^{-n\sigma Y}$, where P/P_0 is the fraction of particles not transmitted through the target, n is the number of atoms per unit volume in the target, σ is the total cross section, and Y is the target thickness. When σ was known, the attenuation factor $A(Y) = 1 - e^{n\sigma Y}$ could be found for each differential thickness Y_i of the target.

To find the net neutron attenuation, a numerical integration was made over the thickness of the target.

Suppose M is the number of μ^--meson stoppings in the target thickness ΔY_i. If g(Y) is the corresponding solid-angle effect, then the net neutron attenuation is

$$A_2 = \frac{\sum_i M(Y_i)\,\Delta Y_i\, g(Y_i)\, A(Y_i)}{\sum_i M(Y_i)\,\Delta Y_i\, g(Y_i)} \quad .$$

The method for finding $M(Y_i)$ and $g(Y_i)$ has already been outlined in Sec. VI. A.

Table III. Results for neutron attenuation in various targets

Elements	A_1	A_2	A_3
S_I	13.34±0.75	2.30±0.13	8.03±0.45
S_{II}	8.28±0.47	2.30±0.13	5.38±0.30
Cu(Solid)	13.92±0.87	2.4 ±0.15	7.86±0.49
Cu(Powder)	13.08±0.82	2.4 ±0.15	7.53±0.47
Ag	8.00±0.76	1.16±0.11	4.47±0.43
Sb (Thin)	6.08±0.38	1.90±0.12	3.23±0.20
Sb (Thick)	12.92±0.82	1.90±0.12	7.63±0.48
Au	8.47±0.80	1.16±0.11	8.47±0.80
Pb	10.61±0.80	1.22±0.092	6.40±0.48
Oxides			
CuO	17.10±0.83	2.28±0.11	11.60±0.56
Sb_2O_3 (Thin)	7.05±0.51	2.06±0.15	3.61±0.26
Sb_2O_3 (Thick)	10.71±0.78	2.06±0.15	6.06±0.44
PbO	8.54±0.77	1.22±0.11	4.96±0.45
Sulfides			
CuS (Powder)	16.09±0.77	3.85±0.20	9.39±0.49
CuS (Cake)	20.41±1.06	3.85±0.20	9.39±0.49
Sb_2S_3	13.47±0.80	2.01±0.12	7.94±0.47
PbS	9.30±0.46	1.55±0.076	5.39±0.26
Metallic Solutions			
AgLi	7.79±1.04	1.43±0.19	4.10±0.56
CuAu	13.31±1.25	1.60±0.15	7.92±0.74

A_1 is the neutron attenuation (in percent) when the neutron source is at the surface of the target. A_2 is the same neutron attenuation expressed in percent per g/cm^2. A_3 is the net neutron attenuation (in percent) when the neutron source is distributed in the target.

VII. RESULTS

This section describes the results for the atomic-capture probabilities of μ^- mesons in the constituents of the compounds as given in Table IV. The C_1 and C_2 represent the atomic-capture probabilities in the higher- and the lower-Z constituent in the compound, respectively. The ratio C_1/C_2 is the relative atomic-capture probability. The sum $C_1 + C_2$ represents the sum of the atomic-capture probabilities and should equal unity. The results have been corrected for both the geometric effect and neutron attenuation.

The summary of results is given in Table V. Assuming the atomic-capture probability goes as Z^n (n being any positive or negative number), we have calculated n for each compound. These are also given in Table V.

Table IV. Results for atomic-capture probability in the constituents of the compounds

Compound	C_1	C_2	C_1/C_2	$C_1 + C_2$
CuAu	0.26±0.023	0.77±0.023	0.34±0.032	1.03±0.032
AgLi	0.921±0.023	0.079±0.023	11.66±3.39	-
CuS†	0.51±0.015	0.27±0.024	1.89±0.18	0.78±0.028
Sb_2S_3	0.59±0.015	0.36±0.020	1.64±0.10	0.95±0.026
PbS†	0.66±0.019	0.23±0.027	2.87±0.35	0.89±0.033
CuO	0.86±0.019	0.14±0.019	6.14±0.85	-
Sb_2O_3	0.65±0.012	0.35±0.012	1.86±0.096	-
PbO	0.82±0.020	0.18±0.020	4.56±0.53	-

The sum $C_1 + C_2$ has not been indicated for AgLi and the oxide compounds because, in these cases, C_2 was calculated from $C_2 = 1 - C_1$ and not independently as in CuAu and sulfide compounds.

† After the atomic captures in oxygen are estimated, the sum is about 0.98 in CuS. The ratio C_1/C_2 remains unchanged. In the case of PbS, the sum changes from 0.89 to 0.94 after estimation of the correction for captures in oxygen. The ratio C_1/C_2 again remains the same. For details see text (Sec. V.C).

Table V. Summary of results. Relative number of μ^- mesons reaching the mesic K shell in the constituents of a chemical compound

Compound	Ratio	Observed	Predicted, Fermi and Teller	Atomic ratio	n
CuAu†	Au/Cu	0.34±0.032	0.495	0.182	0.62±0.094
AgLi†	Ag/Li	11.66±3.39	9.1	0.58	1.08±0.11
CuS	Cu/S	1.89±0.18	1.81	1	1.07±0.16
Sb_2S_3	Sb/S	1.64±0.10	2.13	0.67	0.78±0.053
PbS	Pb/S	2.87±0.35	5.12	1	0.65±0.076
CuO	Cu/O	6.14±0.85	3.62	1	1.41±0.11
Sb_2O_3	Sb/O	1.86±0.096	4.25	0.67	0.55±0.028
PbO	Pb/O	4.56±0.53	10.25	1	0.65±0.050

† AgLi and CuAu are metallic solutions. AgLi has 10% of Li by weight. CuAu has 36% of Au by weight.

VIII. DISCUSSION AND CONCLUSIONS

Suppose the atomic-capture probability for a binary compound is given by $C_1/C_2 = n_1/n_2(Z_1/Z_2)^n$, where C_1 and C_2 are the atomic-capture probabilities for the two constituents of a compound with their atomic concentrations n_1 and n_2, respectively, Z_1 and Z_2 are the atomic numbers, and n is any number that can take positive as well as negative values. For the case considered by Fermi and Teller, n is equal to unity. We have plotted, in Fig. 24, n_2C_1/n_1C_2 versus Z_1/Z_2 for the results obtained from our experiment as well as from previous experiments.[7-13] The results from our experiment fall between $n = 2/3$ and 1.4 over the plot.

Sens et al. remark that their results follow more closely the simple atomic ratios unweighted by the atomic numbers; in fact, a plot of these results shows an inverse Z relationship for the capture process.

Among the metallic compounds examined we notice that AgLi is consistent with n = 1 (Fermi-Teller). Lathrop et al. tested an AgZn alloy in which they showed an agreement of their result with n = 1. A recent measurement of the $CuAl_2$ alloy shows that the atomic μ^--meson capture in Cu occurs at a rate higher than the Z law would predict. The result of Lathrop et al. for AgZn, though compatible with the Z law behavior, is not in disagreement with the $CuAl_2$ result. From the plot, we see that both these results are in agreement with n = 1.5. Therefore, the conclusion of Lathrop et al. that the Fermi-Teller Z law is valid in metallic compounds seems to be an oversimplification. This is further supported by our result for CuAu, which is $n = 2/3$.

Sens et al. point out in their paper that the prediction by Fermi and Teller was based only on their calculation for the energy loss for metals. It had been indicated by Fermi and Teller, themselves, that the energy loss for insulators might be different for metals because the Brillouin gap does not allow arbitrarily small amounts of energy to be transferred from the μ^- meson to the electrons of the insulator.

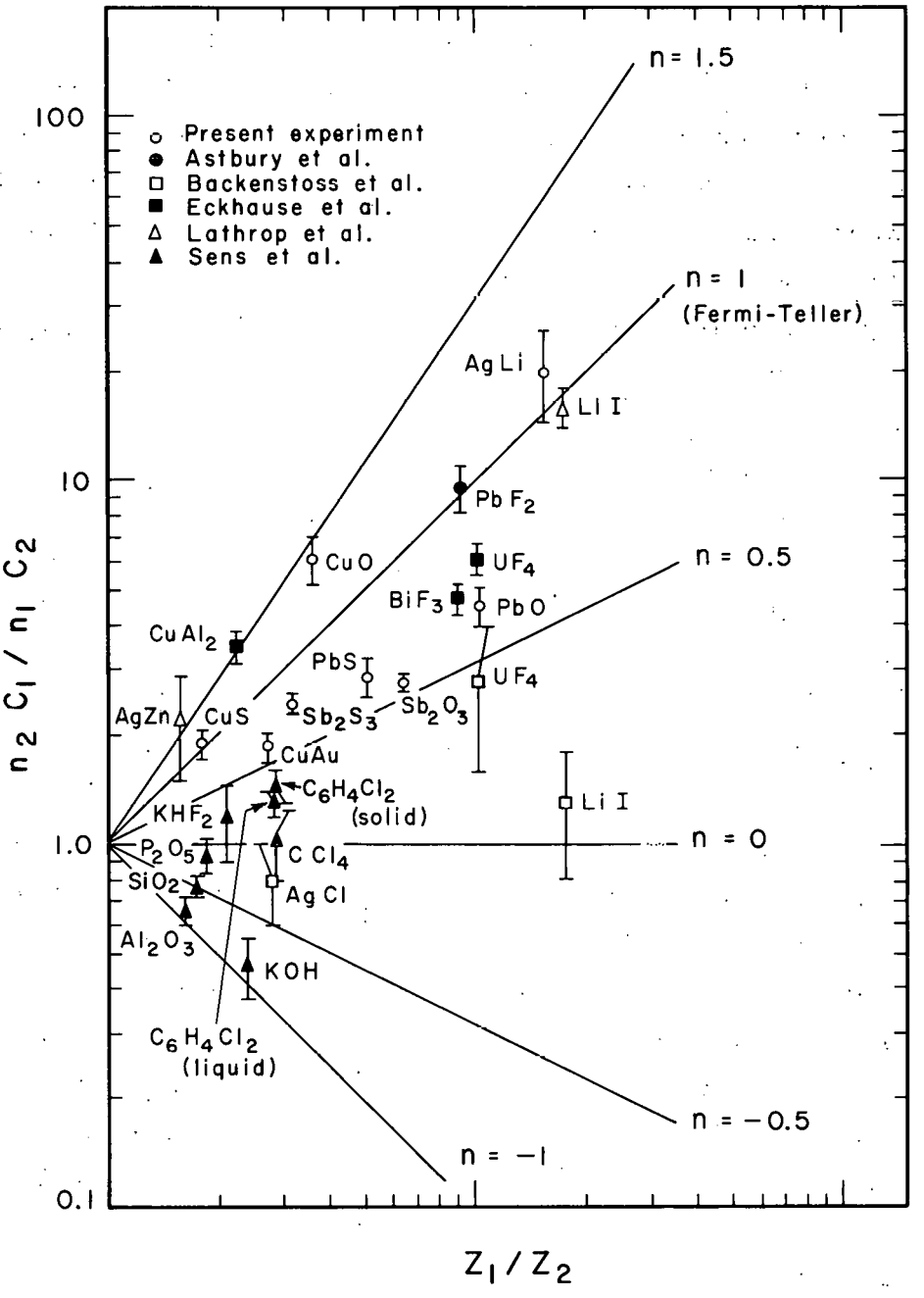

Fig. 24. Plot of $\frac{n_2 C_1}{n_1 C_2}$ vs $\frac{Z_1}{Z_2}$.

When the results of Sens et al., in the case of insulators, showed a disagreement with the Z law behavior, they pointed out that this may be one of the reasons for the breakdown of the prediction by Fermi and Teller. On the basis of the results for metallic solutions and alloys, which also show a departure from the predictions of Fermi and Teller, it appears that, besides the Brillouin gap, there are other features that influence the capture process.

An interesting point to look into would be the possibility that the lattice structure of these compounds has something to do with the μ^--meson captures. The CuAu tested in this experiment had 18% by weight of Au. The metallic solution had a face-centered cubic structure in the disordered state. In the CuAu systems, for more than 18% and less than 47% Au, a superlattice is formed which gives rise to a face-centered cubic structure in the ordered state with Au atoms going to the cube corners and Cu atoms to the face centers.[26] For the atomic percentage between 47 and 53, a tetragonal structure is formed.[26] It might be interesting to study how the capture ratio is affected by a change in the lattice structure for the same compound. In other words, the problem would be to find if the manner in which the different kind of atoms are bound together in the lattice affects the capture ratio. We then might know something about possible energy losses of μ^- mesons to the lattice. Such energy losses, if any, are unknown.

From the plot it is seen that the results for PbO and PbS are described by about the same value of $n \approx 2/3$, while those for CuO and CuS are distributed about $n = 5/4$. It seems to indicate that the compounds that have the same atomic binding may behave in a similar fashion so far as μ^- captures are concerned. We might then expect the same behavior for Sb_2O_3 and Sb_2S_3, but they have large deviations about an average value of $n \approx 2/3$. From Table V it is seen that the results for Sb_2O_3 and Sb_2S_3 have small statistical errors whereas the other compounds have larger errors. It may be that there are some systematic effects in Sb_2O_3 and Sb_2S_3 that make the statistical errors small and, therefore, imply a significant deviation between the n values for these two compounds.

In conclusion, we can say that our experimental results for the relative atomic-capture probability of μ^- mesons in the constituents of a compound fall approximately in the range between $n = 2/3$ and $n = 1.4$. There is thus a positive correlation between the atomic-capture ratio and Z, but not exactly the same as Fermi and Teller predicted. It seems that further theoretical and experimental investigation has to be done before we can arrive at any definite conclusion.

ACKNOWLEDGMENTS

I wish to extend my gratitude to Professor Burton J. Moyer for his guidance and his interest in my work throughout my years of graduate study.

I am extremely indebted to Dr. Selig Kaplan and Dr. Robert V. Pyle for their help and advice in the performance and analysis of the experiment, and without whose help I could not have carried it out. I also wish to thank Justo Diaz and Gabriel Kojoian for their help in the experiment. I am also grateful to the Government of India for awarding me a Central States Scholarship which enabled me to do my graduate study at the University.

This work was done under the auspices of the U. S. Atomic Energy Commission.

APPENDICES

A. Targets

We have described in Sec. I. C the reasons for choosing the different targets used in this experiment. Here we give information relevant to the specific targets.

Target	Thickness (g/cm^2)	Thickness (cm)
Elements		
S	3.6 and 5.8	2.0 and 2.9
Fe	5.9	2.0
Cu (powder)	5.45	2.0
Cu (solid)	5.8	0.645
Ag	6.9	0.66
Sb	3.2 and 6.8	1.0 and 1.6
Au	3 sheets of 50 mil = 7.3	0.38
Pb	8.7	1.2
Metallic Solutions		
AgLi	5.45	1.097
CuAu	8.32	0.752
Insulating Compounds		
A. Sulfides		
CuS	4.18 and 5.3	2.0 and 2.0
Sb_2S_3	6.7	2.0
PbS	6.0	2.5
B. Oxides		
CuO	7.5	2.0
Sb_2O_3	3.42 and 5.2	1.5 and 2.5
PbO	7.0	1.5

B. Capture Rates of μ^- Mesons in Elements

Wheeler showed, on the basis of phenomenological arguments, that the capture rate of negative muons is proportional to the muon density at the position of the nucleus;[28] i.e.,

$$\Lambda_c = \sum_{\text{all protons}} |\psi(0)|^2$$

$$= Z\,|\psi_\mu(0)|^2$$

$$= \frac{Z^4}{\pi a_0^{\,3}} \quad ,$$

where a_0 is the muon Bohr radius and $\psi_\mu(0)$ the K-orbit wave function for the muon at the origin. The approximation of the hydrogenic wave function is not correct for high-Z nuclei, for which the radius of muon orbit is comparable to the nuclear radius. For high-Z nuclei, the capture rate is proportional to Z^4_{eff}, where

$$Z^4_{\text{eff}} = \int |\psi(\vec{r})|^2 \rho(\vec{r})\,d\vec{r} \quad ,$$

where $\psi(\vec{r})$ is the muon wave function normalized so that $\int \psi(r)dr = \pi a_0^{\,3}$, and $\rho(\vec{r})$ is the density function of protons in the nucleus normalized so that $\int \rho(\vec{r})d\vec{r} = Z$. Assuming a uniform nuclear-charge distribution, Wheeler obtained the following interpolation formula for Z_{eff},

$$Z_{\text{eff}} = Z\left[1 + \left(\frac{Z}{37.3}\right)^{1.54}\right]^{-1/1.54} \quad .$$

This formula has been improved by Hillas.[29] Using the recent values of muon mass, nuclear radii, and the proton-density distribution as given by Hill and Ford,[30] he arrived at

$$Z_{eff} = Z\left[1 + \left(\frac{Z}{42}\right)^{1.47}\right]^{-1/1.47}$$

Sens[4] has recalculated Z_{eff} for various nuclei by using the nuclear-charge distributions determined from electron-scattering measurements. The values of Z_{eff} as calculated by Sens are in good agreement with those given by Hillas.

Wheeler's theory predicts larger interaction ratoo for high Z than the experimental values. Primakoff has explained that this disagreement is due to the neutron excess in heavy elements, which reduces the number of momentum states in which the emitted neutron can be accommodated. Using a closure approximation to sum over the final states, Primakoff obtained, for the capture rate,

$$\Lambda_c(A, Z) = (Z_{eff})^4 (\langle\eta\rangle_a)^2 (272\ \text{sec}^{-1}) R\left(1 - \frac{A-Z}{2A}\ \delta\right), \qquad \text{(B-1)}$$

where $\langle\eta\rangle_a$ is the kinematical factor averaged over the final states, R is the ratio of assumed μ^- capture coupling constants to the coupling constant for the β decay of the neutron, $(A - Z_\delta)/2A$ represents a decrease in the capture rate due to the presence of the neutrons in the nucleus occupying final states into which the proton wishes to go, and δ is a nucleon-correlation parameter estimated from nuclear data (its value is 3.0).

Sens[4] has made a least-squares fit of his experimental data to the Primakoff formula. He finds good agreement between theory and experiment. From the least-squares fit, Sens obtained

$$(\langle\eta\rangle_a)^2 (272\ \text{sec}^{-1})\ R = 188\ \text{sec}^{-1}\ \text{(experimental)}$$

$$= 161\ \text{sec}^{-1}\ \text{(theoretical)}. \qquad \text{(B-2)}$$

This provides support for the combination of basic assumptions on which the theory is founded. If the assumption of conserved vector current is abandoned in Primakoff's theory, then

$$(\langle\eta\rangle_a)^2 (272\ \text{sec}^{-1})\ R = 137\ \text{sec}^{-1}\ \text{(theoretical)}. \qquad \text{(B-3)}$$

So it appears that there is a better agreement between theory and experiment if the assumption of conserved vector current is retained.

The agreement between the theoretical and experimental values in (B-2) only tells about the equality of coupling strengths in the two processes but does not reveal anything about the detailed nature of the interaction. It should be pointed out that the Primakoff formula (B-1) gives only a general form of the dependence of the interaction rate on Z.

C. Measurement of Lifetimes and the Capture Rate of μ^- in Elements

In connection with the experiment for testing the Fermi-Teller Z law, it was necessary to measure the lifetimes in a number of elements, namely, S, Fe, Cu, Ag, Sb, Au, and Pb. These measured lifetimes are of statistical accuracy comparable to or greater than the measurements previously reported by other experimenters[3,4,5] (Au has not been measured before). We measured the lifetimes by detecting the capture-product neutrons. For elements with $Z > 10$, the yield for capture products exceeds the decay products. There are very few, if any, background effects caused by mesons stopping in the counter or the container walls. All the earlier measurements have been made by detecting the decay-product electrons. Therefore, the presence of any low-Z material in the immediate neighborhood is a source of relatively large numbers of electrons.

The measured lifetimes have been used to calculate the capture rates in different elements. The total disappearance rate of the μ^- is given by

$$\Lambda_t = \Lambda_d(Z) + \Lambda_c(Z) ,$$

where Λ_t is the total disappearance rate, Λ_d the decay probability, and Λ_c the capture probability.

In our experiment, we determined Λ_t by detecting neutrons, as mentioned in Sec. IV. The data analysis for Λ_t has already been discussed in Sec. V.B. The values of Λ_d were calculated from a theoretical formula given by Huff.[31] The capture rate was calculated from $\Lambda_c = \Lambda_t - \Lambda_d$. The capture rates have been fitted to Primakoff's formula, B-I. The values obtained from the fit are

$$(\langle \eta \rangle_a)^2 (272 \text{ sec}^{-1}) R = 198.2 \pm 5.3$$

and

$$\delta = 3.14 \pm 0.0005. \qquad \text{(B-4)}$$

These values are in agreement with the theory and also with the results of Sens. Figure 25 shows a plot of $\Lambda_{cap}(A, Z)/Z^4_{eff}$ versus A-Z/2A. The straight line is a least-squares fit to the observed data corresponding to the parameters in (B-4). The results are given in Table VI.

Table VI. Average lifetimes for different elements and their capture rates

Element	Average lifetime (nsec)	No. of measure-ments	χ^2	$P(\chi^2)$	Average lifetime after error adjustment (nsec)	$\Lambda_t \times 10^{-5}$ (sec^{-1})	$\Lambda_d \times 10^{-5}$ (sec^{-1})†	$\Lambda_c \times 10^{-5}$ (sec^{-1})
S	498±15	4	3.53	0.30	498±17	20.08±0.69	4.48	15.6±0.69
Cu	162.6±1.21	11	23.75	0.010	162.6±1.9	61.50±0.72	4.39	57.1±0.72
Ag	84.4±0.97	5	1.13	0.90	84.4±1.0	118.48±1.40	4.16	114.3±1.4
Sb	91.3±0.64	16	71.77	$<1.0\times10^{-4}$	91.3±1.4	109.52±1.20	4.12	105.4±1.2
Au	68.6±0.77	8	23.32	4×10^{-4}	68.6±1.3	145.77±2.76	3.80	142.00±2.8
Pb	74.1±0.72	5	10.01	0.05	74.1±1.0	134.95±1.85	3.80	131.2±1.9

† The values of Λ_d have been taken from a paper by Huff.[31]

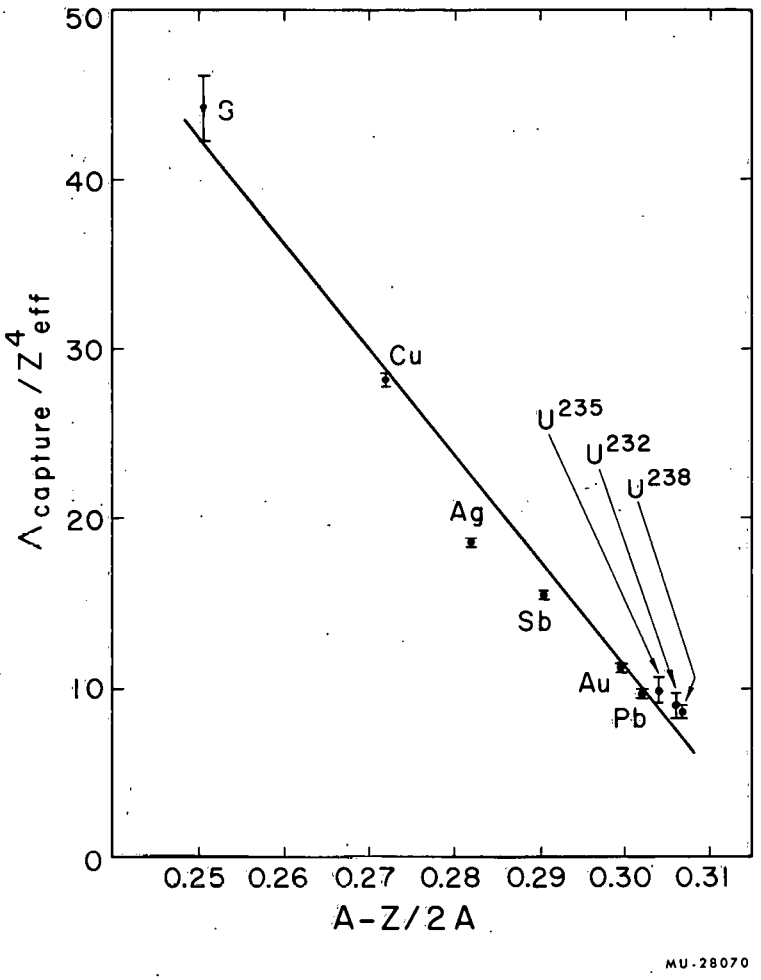

Fig. 25. Plot of $\frac{\Lambda_{capture}(A, Z)}{Z_{eff}^{4}}$ vs $\frac{A-Z}{2A}$. The line is a least-squares fit to the observed data.

Table VII. For the sake of comparison, the lifetimes of μ^- mesons in different elements, from previous workers as well as from our experiment, are given below.

Element	Lifetime (nsec)	Reference
S	498 ± 17	UCRL-10297[32]
	540 ± 20	Sens.[4]
	610 ± 40	Tenner[5]
	700 ± 40	Alberigi-Quaranta et al.[3]
Cu	162.6 ± 1.9	UCRL-10297[32]
	160 ± 4	Sens[4]
	163 ± 6	Holstrom and Keuffel[5]
	155 ± 2	Astbury et al.[5]
	168 ± 7	Gilboy and Tennent[5]
	172 ± 8	Meyer[5]
Ag	84.4 ± 1.0	UCRL-10297[32]
	85 ± 3	Sens[4]
	84 ± 4	Meyer[5]
Sb	91.3 ± 1.4	UCRL-10297[32]
	99 ± 11	Keuffel et al.[3]
Au	68.6 ± 1.3	UCRL-10297[32]
Pb	74.1 ± 1.0	UCRL-10297[32]
	82 ± 5	Sens[4]
	75 ± 3	Meyer[5]
Th†	74.2 ± 5.6	UCRL-10297[32]
U^{235} †	66.5 ± 4.2	UCRL-10297[32]
U^{238} †	75.6 ± 2.9	UCRL-10297[32]
U	88 ± 4	Sens[4]

† For these nuclei, the indication of nuclear capture was a fission fragment rather than a neutron.

REFERENCES

1. M. Tomonaga and G. Araki, Phys. Rev. 58, 90 (1940).
2. M. Conversi, E Pancini, and O. Piccioni, Phys. Rev. 71, 209 (1947).
3. H. K. Ticho, Phys. Rev. 74, 1337 (1948); J. W. Keuffel, F. B. Harrison, T. N. K. Godfrey, and George T. Reynolds, Phys. Rev. 87, 942 (1952); A. Alberigi-Quaranta and E. Pancini, Nuovo Cimento 11, 607 (1954).
4. J. C. Sens, Phys. Rev. 113, 679 (1959).
5. A very good collection of μ^--meson lifetimes in various elements is given in a tabular form by R. M. Tennent in Progress in Elementary Particle and Cosmic Ray Physics (North Holland Publishing Co. Amsterdam, 1960), Vol. 5, p. 386-387.
6. E. Fermi and E. Teller, Phys. Rev. 72, 399 (1947).
7. M. B. Stearns and M. Stearns, Phys. Rev. 105, 1573 (1957).
8. J. C. Sens, R. A. Swanson, V. L. Telegdi, and D. D. Yovanovitch, Nuovo Cimento 7, 536 (1958).
9. M. Rich, and R. Madey, Range-Energy Tables, University of California Radiation Laboratory Report UCRL-2301 (1954).
10. J. F. Lathrop, R. A. Lundy, R. A. Swanson, V. L. Telegdi, and D. D. Yovanovitch, Nuovo Cimento 15, 831 (1960).
11. A. Astbury, P. M. Hatersley, M. Hussain, M. A. R. Kemp, and H. Muirhead, Nuovo Cimento 18, 1267 (1960).
12. G. Backenstoss, B. Block, B. Chidley, R. Reiter, T. Romanowski, R. Siegel, and R. Sutton, Bull. Am. Phys. Soc. II 4, 273 (1959).
13. M. Eckhause, T. A. Fillipas, R. B. Sutton, R. E. Welsh, and T. A. Romanowski, Nuovo Cimento 24, 666 (1962).
14. M. G. Petrashku and A. K. Mikhul, Soviet Physics (Doklady) 4, 628 (1959); ibid., 4, 92 (1959).
15. W. K. H. Panofsky, R. L. Aamodt, and H. Hadley, Phys. Rev. 81, 565 (1951).
16. H. Primakoff, Rev. Mod. Phys. 31, 3 pp. 802-822 (1959).
17. E. Fermi, Z. Physik 48, 73 (1928).

References (cont.)

18. F. D. Brooks, "Organic Scintillators," in Progress In Nuclear Physics, O. R. Frisch, ed. (Pergamon Press, Inc., London, England, 1956) Vol. 5, p. 242-313; and Liquid Scintillation Counting, C. B. Bell and F. N. Hayes, eds. (Pergamon Press, Inc., 1958), p. 268.

19. A Scintillation Counter with Neutron and Gamma Ray Discriminators, Nuclear Instruments and Methods, F. D. Brooks, 4, 151-163 (1959).

20. R. B. Owen, The Decay Time of Organic Scintillators and Their Application to the Discrimination Between Particles of Differing Specific Ionization, IRE trans. on Nuclear Science, Vol. NS-5, pp. 198-201 (1958).

21. M. Forte, Possibilities of Discrimination Between Particles of Different Kinds by Means of Organic Scintillator Decay Curves, in Proceedings of an International Conference on the Peaceful Uses of Atomic Energy, Geneva, September 1958, ALCONF. 15/P/1514.

22. R. B. Owen, Pulse Shape Discrimination, Nucleonics 17, 9, 92 (1959).

23. F. D. Brooks, A Scintillation Counter with Neutron and Gamma-Ray Discriminators, Nucl. Instr. Methods 4, 151-163 (1959).

24. W. Daehnick and R. Sherr, Pulse Shape Discrimination in Stilbene Scintillators, Rev. Sci. Instr. 32, 6, 666 (1961).

25. F. D. Brooks, R. W. Pringle, and B. L. Font, Pulse Shape Discrimination in a Plastic Scintillator, IRE Trans. Nuclear Sci. (1961) p. 35.

26. Structure of Metals, Charles S. Barrett (McGraw-Hill Book Co., Inc., New York, 1952) Ch. XII, p. 269.

27. R. D. Evans, The Atomic Nucleus (McGraw-Hill Book Co., Inc., New York, 1955) pp. 775-77.

28. J. A. Wheeler, Rev. Mod. Phys. 21, 133 (1949).

29. See Ref. 5, p. 399.

30. D. L. Hill and K. W. Ford, Phys. Rev. 94, 1617 (1954).

31. R. W. Huff, Ann. Phys. 16, 288 (1961).

32. Selig N. Kaplan, Jagdish Baijal, Justo A. Diaz, Gabriel Kojoian, and Robert V. Pyle, Lifetimes in Medium and High Z Elements, Lawrence Radiation Laboratory Report UCRL-10297 (1962).